Title: Sigh generation in preBötzinger Complex

Running Title: preBötC Microcircuits for Sighing

Authors:

Yan Cui[1,2,§], ORCID: 0000-0003-1336-1342

Evgeny Bondarenko[2, §], ORCID: 0000-0003-0631-8936

Carolina Thörn Perez[2,3], ORCID: 0000-0002-3480-8599

Delia N. Chiu[2,4], ORCID: 0000-0002-7343-7962

Jack L. Feldman[2*], ORCID: 0000-0003-3692-9412

Affiliations:

1 Department of Physiology, Chengdu Medical College, China

2 Department of Neurobiology, DGSOM, UCLA, Los Angeles, California 90095-1763, USA

3 Gene Expression Laboratory, Salk Institute for Biological studies, La Jolla, CA 92037, USA

4 Synaptic Physiology and Plasticity Group, European Neuroscience Institute Göttingen - A Joint Initiative of the University Medical Center Göttingen and the Max-Planck Society, Göttingen, Germany

***Correspondence**: feldman@g.ucla.edu

§ Co-first authors

Author Contributions J.L.F., Y.C., E.B., C.T.P., and D.N.C. conceived experiments, interpreted data, and wrote the manuscript. Y.C. performed experiments showing the effects on sighing and other aspects of breathing pattern of optogenetic activation of the pF GRP or NMB neurons and preBötC GRPR, NMBR or SST neurons *in vivo*. E.B. performed experiments showing the effects on sighing and other aspects of breathing pattern of chemogenetic excitation and inhibition of preBötC NMBR or SST neurons *in vivo*. C.T.P. performed two-photon calcium imaging experiments showing the activity profiles of preBötC NMBR neurons *in vitro*. D.N.C. performed whole-cell recordings of preBötC NMBR and GRPR neurons *in vitro.* E.B. performed the RNAscope experiments. Y.C., E.B., C.T.P., and D.N.C. analyzed data from their respective experiments.

Acknowledgements: This work was funded by NIH Grants HL135779, NS72211, NSFC Grant 37101012 and Disciplinary Construction Innovation Team Foundation of Chengdu Medical College: CMC-XK-2102.

Abstract

We explored neural mechanisms underlying sighing. Photostimulation of parafacial (pF) neuromedin B (NMB) or gastrin releasing peptide (GRP), or preBötzinger Complex (preBötC) NMBR or GRPR neurons elicited ectopic sighs with latency inversely related to time from preceding endogenous sigh. Of particular note, ectopic sighs could be produced without involvement of these peptides or their receptors in preBötC. Moreover, chemogenetic or optogenetic activation of preBötC SST neurons induced sighing, even in the presence of NMBR and/or GRPR antagonists. We propose that an increase in the excitability of preBötC NMBR or GRPR neurons not requiring activation of their peptide receptors activates partially overlapping pathways to generate sighs, and that preBötC SST neurons are a downstream element in the sigh generation circuit that converts normal breaths into sighs.

53 Introduction

54 Endogenous sighs generated periodically, typically every few minutes in rodents and humans,
55 reinflate collapsed alveoli to maintain proper gas exchange in the mammalian lung[1-3]. Two
56 largely parallel medullary pathways from the parafacial region (pF) to preBötzinger Complex
57 (preBötC) appear critical for generation of these physiological sighs: pF neurons expressing
58 neuromedin B (NMB) or gastrin releasing peptide (GRP) project to preBötC neurons expressing
59 their cognate receptors, NMBR and GRPR[4]. These pathways also appear to mediate
60 confinement-induced claustrophobic sighing[5], and by extension, other forms of sighing
61 associated with emotional states such as during sadness, anxiety, depression, relief, or
62 happiness[6,7].

63 In rodents, the preBötC receives inputs from NMB and GRP pF neurons, and genetic deletion of
64 NMBRs or GRPRs or local antagonism of NMBRs or GRPRs in preBötC significantly reduces
65 endogenous sighing, while local injection into preBötC of bombesin, NMB or GRP significantly
66 increases spontaneous sighing[4]. In order to determine whether NMB and GRP are obligatory for
67 sighs, and to better understand the mechanisms within the preBötC underlying sigh generation,
68 we investigated whether activation of pF NMB or GRP neurons can generate sufficient input to
69 preBötC to induce sighs and whether activation of preBötC GRPRs or NMBRs is necessary for
70 generation of sighs.

71 Using transgenic mice that express Cre- or Flp-recombinase in *Nmb*-, *Grp*-, *Nmbr*- or *Grpr*-
72 expressing neurons, we investigated the effects on sighing and other aspects of breathing
73 pattern *in vivo*: i) of optogenetic activation of ChR2-transfected pF GRP or NMB neurons; ii) of
74 optogenetic or chemogenetic activation of ChR2-transfected preBötC GRPR or NMBR neurons,
75 including in the presence of their antagonists, and; iii) determined whether activating preBötC
76 SST neurons, presumptive preBötC output neurons, can generate sighs. Moreover, by using
77 electrophysiology and two-photon calcium imaging, we investigated the activity profiles of *Grpr*-
78 or *Nmbr*-expressing preBötC neurons *in vitro*.

79 We conclude that: i) activation of either pF NMB or GRP neurons generates sufficient input to
80 preBötC to generate ectopic sighs; ii) sighs can be generated by activation of preBötC GRPR
81 and NMBR neurons even after blockade of NMBR and GRPR receptors; iii) preBötC GRPR or
82 NMBR neurons act via partially overlapping pathways to produce sighs via preBötC SST
83 neurons; iv) preBötC NMBR neurons are not rhythmogenic, and; v) activation of preBötC SST
84 neurons can generate sighs.

85 Results

86 A sigh is an inspiratory effort that results in significantly increased tidal volume (V_T), typically two
87 to five times larger compared to normal breaths with a range of airflow profiles. Here, we define
88 sighs as inspiratory efforts that result in transient significantly (>2-fold) increased V_T, which
89 occur periodically at intervals longer than eupneic, i.e., normal, breaths. For all analyses, we
90 designated sighs by their larger V_T irrespective of their shape. Thus, monophasic 'augmented
91 breaths', biphasic 'partial doublets' or 'full doublets' were all considered sighs (Extended Data
92 Fig. 1). The mechanisms underlying formation of these different sigh subtypes are outside the
93 scope of this publication.

94 **Activation of *Nmb*- or *Grp*-expressing pF neurons induces sighs**

95 To test whether selective activation of pF NMB or GRP neurons, i.e., bombesin peptide-
96 expressing pF neurons) generates sighs, we established Grp-ChR2 or Nmb-ChR2 mouse lines
97 (see *Methods*) by crossing floxed-ChR2-tdTomato mice with Grp^{Cre} and Nmb^{Cre} mice (Fig. 1a,
98 c). We then measured the effects of targeted pF photostimulation (long pulse photostimulation,
99 LPP, single bilateral 4-10 s 5mW pulse or short pulse photostimulation, SPP, single bilateral
100 100-500 ms pulse; see *Methods*)[8] in anesthetized Grp-ChR2 or Nmb-ChR2 mice.

101 In brainstems of adult Grp-ChR2 mice at the rostrocaudal level of the facial nucleus (7N),
102 tdTomato fluorescence is expressed mainly in the dorsomedial part of retrotrapezoid
103 nucleus/parafacial respiratory group (RTN/pFRG; Extended data Fig. 2a), consistent with

104 previous data in newborn mice[4]. In brainstems of adult Nmb-ChR2 mice, Nmb-tdTomato is
105 mainly expressed ventral and lateral to 7N, with a few of these neurons in the 7N, consistent
106 with previous data in mice[9] (Extended data Fig. 2b).

107 In Grp-ChR2 mice, LPP in pF elicited a large breath equivalent to an endogenous sigh in both
108 amplitude and tidal volume (V_T) when initiated during phase 0.3-1.0 of the sigh cycle (see
109 *Methods*); we refer to such events as ectopic sighs (Fig. 1a, bottom). Ectopic sighs in Grp-ChR2
110 mice were of partial doublet or augmented breath shape (See Extended Data Fig.1) and were
111 indistinguishable from endogenous sighs in both V_T and inspiratory (T_I) and expiratory (T_E)
112 duration and exhibited a postsigh apnea (T_E immediately following ectopic sighs increased to
113 216 ± 35% of T_E of eupneic breaths, Fig.1b). During sigh phase 0.3-0.9, the interval from the
114 previous endogenous sigh to the LPP-induced ectopic sigh, i.e., the perturbed sigh cycle, was
115 shorter than the prior control sigh cycle. The interval between an ectopic sigh and the next
116 (endogenous) sigh was, on average, indistinguishable from the interval between endogenous
117 sighs, indicating that ectopic sighs reset the sigh cycle (Fig. 1a). No ectopic sighs could be
118 generated by bilateral pF SPP in Grp-ChR2 mice during inspiration or expiration (phase: 0.0-
119 1.0).

120 In Nmb-ChR2 mice, the effects of pF SPP and LPP were similar to those in Grp-ChR2 mice, as
121 SPP (phase: 0.0-1.0) had no effect on sighing while LPP induced ectopic sighs, which appeared
122 as partial doublet or augmented breaths, and reset the sigh cycle during 0.4-0.9 sigh phase (Fig
123 1c). Ectopic sighs were also indistinguishable from spontaneous sighs in V_T, T_E and T_I and they
124 exhibited a postsigh apnea (T_E after evoked sighs increased to 151 ± 22% of T_E of eupneic
125 breaths, Fig. 1d).

126 Notably, in either Grp-ChR2 or Nmb-ChR2 mice, pF LPP did not elicit ectopic sighs when
127 applied very shortly after an endogenous sigh (phase range: 0.0–0.2 and 0.0–0.3 of
128 endogenous sigh cycle, respectively; Fig. 1e), indicating a postsigh refractory period for sigh

129 induction. LPP in these cases had no subliminal effect on the sigh cycle, as the expected time to
130 the next endogenous sigh was unchanged.

131 When pF LPP was initiated immediately following the end of the postsigh refractory period, the
132 perturbed sigh cycle was significantly shorter than the control sigh cycle. For pF LPP later in the
133 sigh cycle, i.e., closer to when the next endogenous sigh was expected, ectopic sighs occurred
134 at even shorter latencies (Fig. 1e). Thus, after the refractory period during which ectopic sighs
135 could not be elicited, this inverse relationship between photostimulation phase and sigh latency
136 indicated that acute activation of the peptidergic microcircuit was more effective as the sigh
137 phase advanced.

138 **NMBR and GRPR are expressed primarily in excitatory neurons in preBötC**

139 To understand how the activity of peptide-expressing pF neurons results in the generation of
140 sighs, we next examined expression pattern of *Nmbr*- and *Grpr*- expressing cells in the preBötC
141 using fluorescence *in situ* hybridization (FISH; Fig. 2). The vast majority of NMBR and GRPR
142 cells (>97%) did not colocalize with the specific astrocytic marker Aldh1l1, indicating that these
143 cells are neurons (Extended Data Fig. 3). GRPR neurons were present caudal to pF, in a
144 stream continuing dorsocaudally from pF to preBötC. In contrast, with the exception of sparse
145 NMBR/ChAT neurons in nucleus ambiguus (Amb. ~4 neurons in each section) that were
146 excluded from subsequent analysis, NMBR neurons were mainly found in preBötC. As
147 previously reported[4], some neurons coexpressed *Nmbr* and *Grpr* (Fig. 2b). In our sample, 57%
148 of NMBR neurons coexpressed *Grpr*, which constituted 32% of the GRPR population (Fig. 2b,
149 c).

150 Next, we assessed colocalization with the vesicular glutamate transporter VGlut2 to determine
151 whether NMBR and GRPR neurons are glutamatergic. Approximately 85% of NMBR and GRPR
152 neurons co-expressed VGlut2 (Fig. 2b, c). Finally, we asked whether *Nmbr* and *Grpr* were
153 expressed on preBötC SST neurons. We found scant colocalization of SST and NMBR or

154 GRPR (~10%), indicating that the substantial majority of these peptide receptors are not on SST
155 neurons (Fig. 2b, c).

156 **Activation of *Nmbr*- or *Grpr* -expressing preBötC neurons induces sighs**

157 Activation of *Nmb*- or *Grp*-expressing pF neurons generates sufficient input to preBötC to
158 generate ectopic sighs, but is activation of neuropeptide-receptor expressing preBötC neurons
159 via their cognate receptors necessary for sigh production? We tested whether bypassing the
160 peptidergic receptors and directly activating preBötC *Grpr*- or *Nmbr*-expressing neurons could
161 also generate sighs. To do this, we expressed ChR2 or the excitatory DREADD hM3Dq in
162 discrete subsets of preBötC neurons (see *Methods*).

163 To express ChR2 in preBötC GRPR neurons, we microinjected a Flp-dependent ChR2 virus[10]
164 into the preBötC of $Grpr^{Flp}$ mice (Extended data Fig. 2c). While no ectopic sighs could be
165 generated by bilateral preBötC SPP in these mice (phase: 0.0-1.0), preBötC LPP during 0.2–0.9
166 sigh phases elicited ectopic sighs which appeared as partial doublet or augmented breaths, and
167 reset the sigh cycle (Fig. 3a, bottom). Ectopic sighs elicited by preBötC LPP of GRPR neurons
168 were no different from spontaneous sighs in V_T and T_E (Fig. 3b) and exhibited a postsigh apnea
169 (T_E following evoked sighs increased to 194 ± 22%, Fig. 3b).

170 Similarly, in Nmbr-ChR2 mice (Fig. 3c, top), preBötC SPP (phase: 0.0-1.0) had no effect on
171 sighing, while LPP during 0.4-0.9 sigh phases elicited ectopic sighs which appeared as a partial
172 doublet or an augmented breath, and reset the sigh cycle (Fig. 3c, bottom). V_T and postsigh T_E
173 of ectopic sighs were no different from that of spontaneous sighs (Fig. 3d). Ectopic sighs elicited
174 by preBötC LPP of NMBR neurons exhibited a postsigh apnea (postsigh T_E increased to
175 225 ± 33%, Fig. 3d).

176 As with photostimulation of pF NMB and GRP neurons, there was a postsigh refractory period
177 during which we could not generate ectopic sighs in preBötC NMBR or GRPR neurons. Again,
178 the latency from LPP to ectopic sigh onset was inversely related to phase (Fig 3e).

179 We also tested whether activation of preBötC NMBR neurons using an excitatory DREADD
180 could induce sighing. To do this, we transduced preBötC *Nmbr*-expressing neurons by
181 microinjection of Cre-dependent AAV-hM3Dq in $Nmbr^{Cre}$ mice. In these mice, application of the
182 selective agonist clozapine-n-oxide (CNO) to the brainstem surface increased sigh frequency
183 ~threefold (Fig. 3f; see Extended data Fig.4 for control CNO application). Sighs induced by
184 CNO in $Nmbr^{Cre}$ mice were of the doublet shape. Thus, increasing the excitability of preBötC
185 NMBR neurons increases sighing.

186 **preBötC NMBR neurons are rhythmically active**

187 We next asked: what are the electrophysiological properties of the *Grpr*- and *Nmbr*-expressing
188 preBötC neurons? We took several approaches. First, using inspiratory rhythmic slices[11] from
189 neonatal Grpr-EGFP or Nmbr-tdTomato reporter mice, we obtained whole-cell patch-clamp
190 recordings from preBötC GRPR or NMBR neurons while monitoring hypoglossal nerve (XII)
191 inspiratory activity. In Grpr-EGFP mice, only 3 of 21 preBötC GRPR neurons were inspiratory-
192 modulated, i.e., fired during XII inspiratory bursts. In contrast, in Nmbr-tdTomato mice, the
193 majority of preBötC NMBR neurons (10/16) were inspiratory-modulated (Fig. 4a). This finding
194 was confirmed using two-photon calcium imaging of rhythmic slices from Nmbr-GCaMP6f mice,
195 in which we could monitor the activity of up to 10 neurons simultaneously (Fig. 4b). The majority
196 of preBötC NMBR neurons (35/58; n = 6) exhibited inspiratory-modulated Ca^{2+} oscillations
197 coincident with XII bursts (Fig. 4b); however, episodes of non-breathing-modulated episodic
198 bursting, i.e., bursts not in phase with XII, were also seen (Fig. 4c) and varied in frequency from
199 0.025 to 0.1 Hz (Extended Data Fig. 5). Almost all NMBR neurons that had Ca^{2+} elevations
200 during inspiratory bursts also had elevations during sighs (34/35), but not during the pre-I
201 period, consistent with whole-cell recordings (Fig. 4a), indicating that they are likely Type II, i.e.,
202 presumptive non-rhythm generating, neurons[12] (Fig. 4d). The burst duration of the GCaMP6f
203 signal associated with sighs was longer-lasting than those associated with eupneic events in the
204 same neuron (Fig. 4d-e).

205 **NMB converts NMBR neurons inspiratory burstlets into sighs and bursts**

206 In typical recording conditions *in vitro* ($[K^+]_{ACSF}$ = 9 mM), the preBötC population activity burst
207 and the periodic XII discharges are in sync. Under conditions of low excitability ($[K^+]_{ACSF}$ < 7
208 mM), however, in addition to these coincident high amplitude bursts in preBötC and XII, there
209 are low amplitude burstlets in preBötC but not in XII[11]. We have hypothesized that the burstlets
210 represent the rhythmogenic kernel[11,13,14]. NMBR neurons had a Type II firing pattern, i.e., no
211 preinspiratory spiking, suggesting that they are not rhythmogenic.

212 We reliably observed both burstlets and bursts in population activity when we lowered $[K^+]_{ACSF}$ to
213 6 mM[9]. When we did so, NMBR neurons were still active during bursts but never during
214 burstlets (Fig. 4f). When we applied NMB (30 nM), only bursts were observed, while both burst
215 and sigh frequency in both preBötC and XII increased (Fig. 4g). The duration of sighs and
216 eupneic bursts were similar in $[K^+]_{ACSF}$ = 6 mM vs 9 mM (Fig. 4h), while the percentage of sighs
217 increased by 30% during NMB (30 nM) application in 6 mM K^+ (Fig. 4i), similar to the increase
218 elicited by 30 nM NMB at 9 mM K^+ [4].

219 **Activating preBötC GRPR- or NMBR-only neurons has distinct effects on sighing**

220 Photoactivation of preBötC GRPR or NMBR neurons can induce sighs. Given that there are
221 three bombesin-related peptide receptor-expressing subpopulations in preBötC, i.e., neurons
222 that express *Nmbr* but not *Grpr* (NMBR-only), neurons that express *Grpr* but not *Nmbr* (GRPR-
223 only) and neurons that express both *Nmbr* and *Grpr*, does activation of neurons expressing one
224 but not the other of these receptors affect sighs differently? We used an intersectional genetic
225 approach to target neurons that express only one of these receptors, excluding double-positive
226 (GRPR/NMBR) neurons[15]. Thus, using Cre-on/Flp-off and Cre-off/Flp-on viral vectors for the
227 delivery of ChR2 in $Nmbr^{Cre}$;$Grpr^{Flp}$ double mutant mice, we expressed ChR2 in preBötC NMBR-
228 only (Fig. 5a) or GRPR-only neurons (Fig. 5d), respectively. We examined the effect of preBötC
229 LPP and SPP of these neurons on sighing. When targeting NMBR-only neurons, preBötC SPP
230 elicited ectopic bursts which appeared similar to partial doublets or augmented breaths with
231 smaller V_T compared to spontaneous sighs due to a decrease in T_I to 64 ± 8% (Fig. 5c). T_E
232 immediately following these ectopic bursts were longer than the T_E of eupneic breaths (Fig. 5c).

233 Note that the time between the SPP-induced ectopic burst and the next endogenous sigh was
234 shorter than the time between endogenous sighs, indicating that SPP-induced burst did not
235 reset the sigh cycle (Fig. 5b, top); SPP-induced ectopic burst could also occur in a sigh
236 refractory period right after the previous eupneic sigh (Fig. 5b, bottom). When targeting GRPR-
237 only neurons, while ectopic sighs could not be generated by SPP at any phase of the sigh cycle,
238 preBötC LPP in the late phase of the sigh cycle elicited ectopic sighs with a partial doublet or
239 augmented breath shape and reset the sigh cycle (Fig. 5e). T_I, T_E and V_T of LPP-induced sighs
240 were indistinguishable from spontaneous sighs (Fig. 5f). The ectopic sighs exhibited a postsigh
241 apnea, T_E after evoked sighs increased to 171 ± 12% of the T_E of eupneic breaths (Fig. 5f).

242 These data suggest that GRPR and NMBR neurons play different overlapping roles in sigh
243 generation.

244 **Activating preBötC GRPR or NMBR neurons has distinct effects on inspiratory burst**
245 **amplitude**

246 In addition to generating sighs, activation of preBötC NMBR and/or GRPR neurons also affected
247 eupneic breathing frequency (*f*) and V_T. In $Grpr^{Flp}$ mice expressing ChR2 in preBötC, LPP during
248 the sigh refractory period did not generate ectopic sighs but increased *f* to 131 ± 9% of baseline
249 (Fig. 6a), and increased V_T to 117 ± 4% of baseline (Fig. 6a), however, when excluding double-
250 positive (GRPR/NMBR) neurons, preBötC SPP or LPP of GRPR-only neurons did not change
251 the inspiratory burst amplitude in stimulus cycles (Fig. 6b).

252 In contrast, in Nmbr-ChR2 mice, preBötC LPP delivered during a postsigh refractory period did
253 not generate ectopic sighs but decreased *f* to 83 ± 4% (Fig. 6a) and increased V_T to 140 ± 12%
254 (Fig. 6a) of baseline. preBötC SPP or LPP of NMBR-only neurons increased V_T to 274 ± 41% or
255 264 ± 17% of control, respectively (Fig. 6b).

256 The effect on inspiratory burst amplitude was also observed in $Nmbr^{Cre}$ mice that had preBötC
257 NMBR neurons transfected with Cre-dependent AAV-HM3Dq; CNO applied to the brainstem

258 surface significantly increased V_T by 343 ± 56% (Fig. 6c) and decreased *f* by 63 ± 8.4% (Fig.
259 6c). Note that although such breaths were of the same V_T as eupneic sighs before
260 administration of CNO (Fig.3c), in line with our definition of sighs (Extended Data Fig.1), we
261 classify this outcome as large amplitude breaths rather than "all sigh" breathing rhythm,
262 according to our definition of sighs (Extended Data Fig.1).

263 Thus, stimulation of preBötC NMBR and/or GRPR neurons also has a profound effect on the
264 eupneic, nonsigh, breathing pattern, and GRPR and NMBR neurons appear to differently affect
265 inspiratory burst amplitude.

266 **Sighs can be induced after inhibition of GRPRs or NMBRs**

267 Expression of *Grpr* and/or *Nmbr* defines subsets of preBötC neurons that affect sigh generation.
268 Is activation of these peptide receptors *necessary* for sigh generation?

269 For that we investigated the effects of activating peptide-expressing pF neurons in the presence
270 of bombesin receptor antagonists. First, we confirmed that bilateral microinjection of the NMBR
271 antagonist BIM23042 and GRPR antagonist RC3095 (300 μM each, 50 nl/side) into the preBötC
272 in anesthetized mice eliminates spontaneous sighs (Extended Data Fig. 6). Next, we
273 determined the effects of such NMBR and GRPR antagonism on LPP-evoked sighs. After
274 blockade, no sighs were elicited by pF LPP in Nmb-ChR2 mice; in contrast, pF LPP of GRP
275 neurons still elicited ectopic sighs of a doublet shape. The V_T was not significantly different from
276 that of spontaneous sighs; T_E of the following respiratory cycle was unaffected (Fig. 6d). Thus,
277 when pF NMB neurons were stimulated, preBötC NMBR neurons require NMBR activation to
278 contribute to sigh generation, whereas when pF GRP neurons were stimulated, sighs could still
279 be generated after antagonism of preBötC GRPR receptors.

280 We next investigated whether explicit activation of preBötC NMBRs and/or GRPRs is necessary
281 to produce sighs, i.e., could sighs be generated simply by depolarizing these preBötC neurons
282 to fire action potentials? In ChR2-transduced $Grpr^{Flp}$ or Nmbr-ChR2 mice after antagonism of

283 both receptors sufficient to eliminate spontaneous sighs (Extended Data Fig. 6), LPP of preBötC
284 GRPR or NMBR neurons still elicited sighs of doublet shape. V_T and T_I of the sighs elicited in
285 $Grpr^{Flp}$ or Nmbr-ChR2 mice after blockade of both receptors was no different from spontaneous
286 sighs (Fig. 6d). Postsigh apnea was observed in $Grpr^{Flp}$ (T_E immediately following the sigh
287 increased to 132 ± 24%), but not in Nmbr-ChR2 mice (Fig. 6d).

288 Thus, initiating or increasing the activity of pF GRP neurons, or preBötC GRPR or NMBR
289 neurons, can generate sighs without activation of these receptors, either endogenously or
290 exogenously.

291 **preBötC SST neurons mediate sighing**

292 Can activity of preBötC neurons other than those expressing *Grpr* or *Nmbr* generate sighs? To
293 address this question, we virally expressed ChR2 (Fig. 7a), hM3Dq (Fig. 7e), or the PSAM4
294 (Fig. 7g) in preBötC SST neurons. In ChR2-transduced Sst^{Cre} mice, bilateral preBötC SPP
295 during inspiration elicited ectopic sighs of partial doublets or augmented breath shapes and
296 reset the sigh cycle (Fig. 7b). V_T, T_I and T_E of the induced sighs were no different from those of
297 spontaneous sighs (Fig. 7c). The ectopic sighs elicited by photostimulation of preBötC SST
298 neurons exhibited a postsigh apnea, T_E of the following respiratory cycle increased by
299 210 ± 19% (Fig. 7c). After BIM23042 and RC3095 microinjection (300 μM each, 50 nl/side),
300 spontaneous sighs were eliminated (Extended Data Fig. 6). In the presence of antagonists,
301 preBötC SPP during inspiration could still elicit an ectopic sigh (Fig. 7d). V_T and T_I of ectopic
302 sighs elicited after blockade of both receptors were no different from spontaneous sighs, or from
303 ectopic sighs elicited before blockade (Fig. 7c). Ectopic sighs elicited after blockade also had a
304 postsigh apnea, T_E of the following respiratory cycle increased by 236 ± 49% (Fig. 7c).

305 In hM3Dq-transduced Sst^{Cre} anesthetized mice (Fig. 7e), excitation of preBötC SST neurons by
306 CNO application onto ventral brainstem surface affected eupneic breathing: *f* decreased by
307 60 ± 6.2%, V_T increased by 222 ± 21%. CNO application increased sigh rate ~tenfold with sighs

308 appearing as doublets (Fig. 7f). In these mice, subsequent microinjection of BIM23042 and
309 RC3095 into preBötC did not affect *f*, V_T or sigh rate induced by CNO administration (Fig. 7f).
310 Thus, excitation of preBötC SST neurons can produce sighs in an NMBR- and GRPR-
311 independent manner.

312 Next, we investigated whether sighs induced by the NMBR- and GRPR-dependent pathway
313 requires activity of preBötC SST neurons. For that we transfected preBötC SST neurons with
314 Cre-dependent ultrapotent inhibitory DREADD AAV-PSAM4-GlyR[16] in Sst^{Cre} mice (Fig. 7g). The
315 sigh rate was then increased by microinjection of peptides NMB and GRP (250 μM each, 50
316 nl/side) into preBötC (Fig.7g, h) in ketamine/xylazine anesthestized mice, which also decreased
317 *f*, and increased V_T (Fig.7g, h). Subsequent application of the PSAM4-GlyR ligand uPSEM817
318 to the brainstem surface did not affect *f* or V_T, but completely eliminated all sighs (Fig.7g, h).
319 Note that similar to excitatory DREADD effects in $Nmbr^{Cre}$ mice, manipulations increasing V_T of
320 all breaths were classified to affect V_T of eupneic breaths rather than induce an “all sigh” rhythm,
321 according to our definition of sighs (Extended Data Fig.1).

322 ## Discussion

323 In all mammals, sighs are generated periodically to maintain lung function and, in humans, are
324 episodically associated with such emotional states as relief, sadness, yearning, exhaustion,
325 stress, and joy[1-3,6,7], and in rodents are associated with inferred indicators of emotional states
326 such as stress and anxiety[17]. The signals producing these large periodic inspiratory efforts
327 originate within the preBötC, a heterogeneous medullary population that is the kernel for
328 generation of breathing rhythm[18]. Molecularly-defined preBötC subpopulations underlie different
329 functions during breathing[18]. Ablation, genetic deletion or pharmacological excitation or
330 inhibition of preBötC neurons expressing receptors (NMBR and GRPR) for bombesin-related
331 peptides (NMB and GRP) significantly affect rhythmic (~25-40/hour) sighing in rodents[4]. Here,
332 we further explored the mechanisms of sigh generation.

333 Sighs exhibit various shapes, i.e., augmented single inspiratory effort, partial doublets, and full
334 doublets, that have two unifying characteristics: i) significant transient increase in V_T and;
335 ii) occur at a much lower frequency compared to eupneic breaths; often these augmented
336 inspiratory efforts are followed by a lengthened interburst interval, i.e., postsigh apnea. We use
337 these criteria as a definition of sighs, which unifies observations and conclusions in this and
338 previous *in* vivo[6,17,19,20] and *in vitro*[21,22] studies that used various, often incongruent definitions of
339 sighs.

340 Here, we investigated two novel properties of sigh generation: sigh phase and postsigh
341 refractory period. By using the same approach that we employed for differentiating the effects of
342 optogenetic stimulation on various preBötC subpopulations on the eupneic cycle[8,20,23], we found
343 that sighs evoked by optogenetic stimulation of various subpopulations reset the sigh cycle and
344 delayed the onset of the next endogenous sigh. Also, similar to a postinpiratory refractory period
345 in the respiratory cycle, during which ectopic breaths cannot be evoked immediately following
346 termination of an inspiratory effort[8], we similarly observed a postsigh refractory period following
347 an endogenous sigh, during which ectopic sighs could not be evoked. We suggest that these
348 subpopulations have intrinsic "sigh-generating" properties, e.g., unique signaling pathways or
349 connectivity that affects excitability of these subpopulations. Although vagotomy transiently
350 abolishes eupneic sighs[24], they can be evoked in absence of sensory feedback *in vivo* after
351 vagotomy[25] or *in vitro*[21,22], suggesting that sensory inputs by themselves are not necessary, but
352 likely modulate activity of these subpopulations to affect frequency of sighs. The mechanisms
353 that underlie the slow sigh rhythm (~minutes) remains to be discovered, and might involve
354 intracellular Ca^{2+} oscillations[26].

355 In mice, sigh-like movements appear *in utero* between E17 and E18[27], when at least two types
356 of inspiratory-modulated neurons can be differentiated in rhythmic slices: neurons that fire in
357 sync with regular "eupneic" XII bursts, and those that fire only during sigh-like bursts[27]. This
358 could result from increased activity in a single population with a distribution of activation
359 thresholds or from recruitment of a distinct high threshold population. *In vitro*, the majority of

360 NMBR preBötC neurons recorded were active in both eupneic and sigh bursts, a few GRPR
361 preBötC neurons recorded were active in eupnea, but none were active exclusively during
362 sighs, q.v.,[27]. Rhythmic preBötC NMBR neurons in neonatal mice were active during both
363 eupneic and sigh bursts (Fig. 4b), but not during burstlets or the pre-I period. These results
364 suggest that NMBR preBötC neurons are Type II neurons that participate in generation of the
365 burst patterns of sighs and eupneic breaths, but are not rhythmogenic.

366 Sighs can be induced by activation of various subpopulations within two structures: NMB or
367 GRP in pF and NMBR, GRPR or SST in preBötC. We previously reported a microcircuit capable
368 of generating sighs involving pF neurons producing bombesin-related peptides that project to
369 preBötC neurons expressing cognate NMBRs and GRPRs[4], and that activation of these
370 preBötC neurons via their peptide receptors was sufficient to generate sighs[4]. Here, in
371 significantly extending this work, we show that sighs can be evoked by direct photoexcitation of
372 GRP, NMBR or GRPR neurons, bypassing activation of these receptors. Photostimulation of
373 preBötC GRPR or NMBR neurons can elicit ectopic sighs (Fig. 3a and 3c), even in the presence
374 of GRPR and NMBR antagonists at sufficient concentration to block the effect of exogenous
375 application of peptides that increase sigh rate (Fig. 6d and Extended data Fig. 6). Thus, sighs
376 can be induced by increasing the excitability of these subpopulations, without obligatory
377 participation of pathways activated by bombesin-related peptides. In other words, while it can
378 provide sufficient external input to trigger sighs, activation of preBötC NMBRs and/or GRPRs is
379 not necessary for sigh production. This suggests that sighs are not the unique product of a
380 preBötC bombesin-peptide signaling pathway.

381 We studied photoactivation of pF NMB- and GRP-expressing neurons in transgenic mice. Could
382 our protocol have also activated GRP or NMB containing presynaptic terminals originating from
383 brainstem neurons outside pF, such as found in the parabrachial nuclei and NTS[4]? This is
384 unlikely in the case of NMB, since NMB-expressing neurons are limited to pF in the medulla[4].
385 Also, unlikely the case of GRP, as there is no evidence that pF neurons express GRPRs[28].
386 However, our protocol would result in the expression of ChR2 in neurons that expressed NMB-

387 or GRP-expressing neurons at any point since conception, even transiently. Thus, we cannot
388 rule out that; in our adult mice there were neurons in pF that once expressed these peptides but
389 no longer did so, and that these vestigial NMB or GRP neurons could have been perturbed in
390 our protocol. Such determination requires additional studies outside the scope of the work
391 reported here.

392 preBötC neurons expressing SST, mostly distinct from NMBR and GRPR populations (Fig. 2),
393 receive input from rhythmogenic preBötC neurons, many have an inspiratory firing pattern[14],
394 that appear to serve a premotor role to shape inspiratory motor output[8]. Photostimulation of
395 preBötC SST neurons increases peak inspiratory amplitude in both anesthetized and awake
396 mice[8,23]. Here, DREADD-mediated excitation of SST neurons significantly increased sigh rate,
397 with the effect much larger than DREADD-mediated excitation of NMBR neurons (16- vs 3-fold
398 increase). Additionally, unlike the significant 1-5s latency to induce an ectopic sigh when
399 photostimulating GRPR or NMBR preBötC neurons (Fig. 3e), photostimulating preBötC SST
400 neurons during inspiration induced a second augmented inspiration immediately following the
401 eupneic burst to convert it into a sigh (Fig. 7b). Importantly, effects of such photostimulation
402 were unaffected by blockade of both NMBR and GRPR receptors (Fig.7d), and sighs evoked by
403 microinjection of peptides NMB and GRP into preBötC were completely eliminated by inhibition
404 of SST neurons that expressed an inhibitory DREADD PSAM4 (Fig. 7g and 7h). We conclude
405 that activation of preBötC SST neurons is also sufficient to induce sighs and further suggest
406 they can induce sighs, downstream from NMBR and GRPR preBötC neurons, and may be
407 necessary to do so (Fig. 8).

408 Our initial delineation of a microcircuit of four subpopulations, i.e., pF NMB and GRP neurons
409 and preBötC NMBR and GRPR neurons, that affected sighs led us to hypothesize its role in
410 sigh generation, but we were agnostic as to its role in the production of eupneic breaths[4]. Our
411 data here, consistent with a previous report of effects from intravenous administration of
412 bombesin[29], suggests that this microcircuit is tightly integrated within the eupneic CPG with
413 NMBR, GRPR and SST populations having distinct though overlapping roles in modulation of

414 the eupneic breathing pattern as well as in the generation of sighs. The majority of preBötC
415 neurons expressing NMBR, GRPR (or both) receptors are glutamatergic and excitatory (Fig. 2).
416 *In vitro*, no NMBR preBötC neurons were active during burstlets or the pre-I period, suggesting
417 that NMBR preBötC neurons are Type II neurons that participate in generation of breathing
418 pattern but not rhythm generation (similar to the properties of preBötC SST neurons[14]). *In vivo*
419 we observed distinctly different effects from activation of preBötC GRPR and NMBR neurons:
420 photoactivation of GRPR neurons increased breathing frequency, whereas photo- or chemo-
421 activation of NMBR neurons decreased breathing frequency and increased amplitude (Fig. 6a
422 and 6c); otherwise, their effects on sighing appeared similar (Fig. 3). Notably, some neurons
423 express both NMBR and GRPR receptors (Fig. 2). When the overlapping subpopulation of
424 preBötC neurons expressing both GRPRs and NMBRs was excluded, we could activate the two
425 discrete pathways independently. Photostimulating GRPR-only neurons had no effect on
426 inspiratory burst amplitude, whereas photostimulating NMBR-only neurons increased amplitude
427 (Fig. 6b). Additionally, DREADD-mediated excitation of the SST population increased both the
428 sigh rate and the inspiratory burst amplitude (Fig. 7f). Microinjection of peptides NMB and GRP
429 into preBötC increased sigh rate and inspiratory burst amplitude; subsequent ultrapotent
430 chemogenetic inhibition of preBötC SST^+ neurons selectively abolished sighs, but not an
431 increase in inspiratory amplitude (Fig. 7g and 7h), suggesting that modulation of breathing
432 pattern by NMBR and GRPR neurons is independent of SST neurons (Fig. 8).

433 Sighing is a relatively straightforward behavior that appears to result from a delineable
434 microcircuit that could only be discovered because of the close relationship between the
435 essential, readily localizable, compact circuitry with a definitive precisely measurable functional
436 physiologically relevant output. How this unexpected complexity for sigh generation reflects on
437 strategies for unraveling ever more complex and difficult to quantify behaviors remains to be
438 determined.

439

440 Methods

441 Experimental procedures were carried out in accordance with the United States Public Health
442 Service and Institute for Laboratory Animal Research Guide for the Care and Use of Laboratory
443 Animals. All animals were handled according to institutional protocols at the University of
444 California, Los Angeles (#1994-159-83P0) and approved by University of California Animal
445 Research Committee (Animal Welfare Assurance #A3196-01). Every effort was made to
446 minimize pain and discomfort, as well as the number of animals.

447 **Animals**

448 Grp^{Cre} was obtained from Jackson Labs (Strain #033174). $Grpr^{flp}$, Nmb^{Cre} and $Nmbr^{Cre}$ animals
449 were designed and generated by Cyagen Biosciences Inc (see below). Transgenic ChR2 mice
450 were generated by crossing Cre mice with floxed-ChR2-tdTomato mice (Jackson Labs Strain
451 #012567). These crosses generated mice expressing ChR2 in GRP neurons (Grp-ChR2), NMB
452 neurons (Nmb-ChR2) or NMBR neurons (Nmbr-ChR2). To express ChR2 selectively in preBötC
453 neurons, AAV injections were performed on adult Sst^{Cre} mice (Jackson Labs Strain #013044) or
454 $Grpr^{flp}$ mice. All *in vivo* experiments were performed on adult male or female mice (10-14 weeks
455 old, 24-32g). Unless otherwise specified, mice were anesthetized with ketamine/xylazine. For *in*
456 *vitro* experiments, transgenic Grpr-EGFP, Nmbr-tdTomato, and Nmbr-GCamp6s were used.
457 These mice were generated by crosses between $Nmbr^{Cre}$ or $Grpr^{Flp}$ mice and one of the
458 following lines: Ai14 (Jackson Labs Strain #007914), RCE:FRT (MMRRC Strain #032038-JAX),
459 GCaMp6f (Jackson Labs Strain #029626).

460 To generate Nmb^{Cre} mice the open reading frame of Cre recombinase together with SV40 polyA
461 signal was cloned downstream of the mouse Nmb promoter, such that the expression of Cre
462 mimicked the endogenous mouse Nmb gene. The PiggyBac ITRs was inserted into the BAC
463 backbone flanking the genomic insert, to facilitate transposes mediated BAC integration. The
464 modified BAC was co-injected with transposes into single cell stage fertilized eggs from
465 C57BL/6 mice. Resulting pups were then genotyped by PCR for the presence of the modified

466 BAC and the Cre cassette. To generate Grpr^{Flp} mice, the Grpr gene was first located on mouse
467 chromosome X. Three exons have been identified, with the ATG start codon in exon 1 and TAG
468 stop codon in exon 3; the TAG stop codon was then replaced with the Flp cassette. To engineer
469 the targeting vector, homology arms were generated by PCR using BAC clone RP23-402H23
470 and RP23-50M18 from the C57BL/6J library as template. In the targeting vector, the Neo
471 cassette was flanked by FRT sites. DTA was used for negative selection. The constitutive
472 knock-in allele was obtained after FRT-mediated recombination. C57BL/6 ES cells were then
473 used for gene targeting to introduce knock-in alleles into host embryos followed by transfer into
474 surrogate mothers. Resulting pups were then genotyped by PCR for the presence of the Flp
475 cassette. To generate Nmbr^{Cre} mice, the Nmbr gene was first located on mouse chromosome
476 10. Three exons have been identified, with the ATG start codon in exon 1 and TGA stop codon
477 in exon 3; the TGA stop codon was then replaced with the Cre cassette. To engineer the
478 targeting vector, homology arms was generated by PCR using BAC clone RP24-232I16 and
479 RP24-124K10 from the C57BL/6J library as template. In the targeting vector, the Neo cassette
480 was flanked by LoxP sites. DTA was used for negative selection. The constitutive knock-in allele
481 was obtained after Cre-mediated recombination. C57BL/6 ES cells were then used for gene
482 targeting to introduce knock-in alleles into host embryos followed by transfer into surrogate
483 mothers. Resulting pups were then genotyped by PCR for the presence of the Cre cassette.

484 **Viral vector design**

485 pAAV-hSyn Con/Foff hChR2(H134R)-EYFP (Addgene plasmid # 55646 ;
486 http://n2t.net/addgene:55646 ; RRID:Addgene_55646) and pAAV-hSyn Coff/Fon
487 hChR2(H134R)-EYFP (Addgene plasmid # 55648 ; http://n2t.net/addgene:55648 ;
488 RRID:Addgene_55648) were gifts from Karl Deisseroth[15]. pAAV-hSyn-DIO-hM3D(Gq)-mCherry
489 was a gift from Bryan Roth (Addgene plasmid # 44361; http://n2t.net/addgene:44361;
490 RRID:Addgene_44361). pAAV-Syn-flex-PSAM4-GlyR-IRES-EGFP was a gift from Scott
491 Sternson[16] (Addgene plasmid # 119741; http://n2t.net/addgene:119741;
492 RRID:Addgene_119741). All viruses were stored in aliquots at -80°C until use.

493 **Viral injections**

494 Mice were anesthetized with isoflurane (4% for induction and 2% for maintenance) and placed
495 in a stereotaxic apparatus (David Kopf Instruments) with Bregma and Lambda skull landmarks
496 level. Two holes were drilled in the skull 6.80 mm caudal to Bregma and 1.2 mm lateral to the
497 midline. Virus was delivered 4.65 mm from the dorsal surface of the brain into the preBötC
498 through a glass pipette using either a pressure ejection system (Picospritzer II; Parker Hannafin)
499 or Micro4 microinjection system (World Precision Instruments). For ChR2 experiments, we used
500 100-200 nl of virus solution (1-6 x 10^{12} vg/ml) per side, and for DREADD experiments, 30-50 nl
501 of virus solution (4.6 x 10^{12} vg/ml) per side. The pipettes were left in place for 5 min after
502 injection to minimize backflow. The wound was closed with 5-0 gauge non-absorbable sutures.
503 Mice were returned to their home cage and given 2-3 weeks to recover to allow for sufficient
504 levels of protein expression. All virus injection sites were subsequently confirmed by
505 immunostaining and only mice with sufficient and localized transfection in preBötC were used
506 for all analysis (see Extended Data Fig. 2 for representative confocal images).

507 **Surgical procedures for ventral approach**

508 Adult mice were anesthetized via intraperitoneal injection of ketamine and xylazine (100 and 10
509 mg/kg, respectively). Isoflurane (1-2% volume in air) was administered throughout an
510 experiment. The level of anesthesia was assessed by the suppression of the withdrawal reflex.
511 A tracheostomy tube was placed in the trachea through the larynx, and respiratory flow was
512 detected with a flow head connected to a transducer to measure airflow (Mouser Electronics).
513 The mice were placed in a supine position in a stereotaxic instrument (David Kopf Instruments).
514 The larynx was denervated, separated from the pharynx, and moved aside. The basal aspect of
515 the occipital bone was removed to expose the ventral aspect of the medulla. The canal of the
516 hypoglossal nerve (XII) served as a suitable landmark. The preBötC were 0.15 mm caudal to
517 the hypoglossal canal, 1.2 mm lateral to the midline, and 0.24 mm dorsal to the ventral
518 medullary surface.

519 **Photostimulation**

520 A 473 nm laser (OptoDuet Laser; IkeCool) was targeted bilaterally to the preBötC or pF with a
521 branching fiber patch cord (200 µm diameter; Doric Lenses) brought to the exposed ventral
522 medullary surface. Laser power was set at 5 mW. Short Pulse Photostimulation (SPP; 200 ms)
523 and Long Pulse Photostimulation (LPP; 5 s) waveforms were delivered under the command of a
524 pulse generator (Pulsemaster A300 Generator; WPI) connected to the laser power supply. In
525 instances where breathing frequency was decreased, e.g. after BIM23042 and RC3095
526 microinjections, SPP and LPP of longer durations (500 ms and 8 s, respectively) were used to
527 confirm consistency of results. Stimulating 500 µm rostral to preBötC or pF in mice expressing
528 ChR2 that served as a control did not produce significant output effects (Extended data Fig. 7b).
529 No output effects and no sigh were produced by preBötC or pF photostimulation in Grp-RFP,
530 Grpr-EGFP, Nmbr-EGFP, Nmb-RFP reporter mice (Extended data Fig. 7a).

531 **Pharmacological injection experiments**

532 The NMBR antagonist BIM23042 (Tocris Bioscience) and the GRPR antagonist RC3095
533 (Sigma-Aldrich) were injected together (300 µM each, 50-60 nl/side) to block NMBR and GRPR
534 activation. Injections were made using micropipettes (~40 µm tip), placed bilaterally into the
535 preBötC. Injections targeted to the center of the preBötC were placed 0.15 mm caudal to the
536 hypoglossal canal, 1.2 mm lateral to the midline, and 0.24 mm dorsal to the ventral medullary
537 surface[8]. Small corrections were made to avoid puncturing of blood vessels on the surface of
538 the medulla. All injections were made using a series of pressure pulses (Picospritzer, Parker-
539 Hannifin; or Micro4, World Precision Instruments). For activation of hM3Dq receptors, 50µL of
540 CNO solution was applied to the ventral surface of the brainstem. CNO (Tocris Biosciences)
541 was dissolved in saline at concentration of 1 mg/ml with 0.5% dimethylsulfoxide. Solution was
542 prepared fresh daily. For activation of PSAM4-GlyR receptors, 30µL of uPSEM817 tartrate
543 solution (10mM) was applied to the ventral surface of the brainstem. In chemogenetic
544 experiments CNO or uPSEM817 were applied to the ventral surface of the brainstem instead of

545 microinjection in order to avoid preBötC damage from multiple microinjections; in control
546 experiments application of the same dose of CNO or uPSEM817 does not produce responses in
547 any breathing parameters.

548 ***In situ* hybridization and immunostaining**

549 $Nmbr^{Cre}$, SST^{Cre} or wild-type mice (10-14 weeks) were euthanized with isoflurane overdose,
550 their brainstems were rapidly removed and flash frozen in dry ice. Fresh frozen brainstems were
551 sectioned sagittally on a cryostat (CryoStar NX70, Thermo Scientific), mounted on SuperFrost
552 Plus slides (Fisher Scientific) and stored at -80℃ for at least 1 day. They were then processed
553 according to manufacturer's protocol (RNAscope version 1, Advanced Cell Diagnostics). Briefly,
554 tissue samples were postfixed in 10% neutral buffered paraformaldehyde, washed, and
555 dehydrated in sequential concentrations of ethanol (50, 70, and 100%). Samples were treated
556 with protease IV and incubated for 2 hours at 40℃ in HybEZ™ Hybridization Oven (Advanced
557 Cell Diagnostics) in the presence of target probes. We used combinations of following probes
558 for hybridization: *Mm-ChAT*, *Mm-Grpr, Mm-Nmbr, Mm-Sst*, *Mm-Slc17a6 (VGluT2), Mm-Aldh1l1,*
559 *Cre* and *Flp*. A probe for *Mm-ChAT* was used in all probe combinations to mark the location of
560 nucleus ambiguus, which is necessary for determining the location of preBötC. After a 4-step
561 amplification process, samples were counterstained with DAPI and coverslipped with ProLong
562 Gold (Invitrogen) used as a mounting agent. Images were acquired on a confocal laser
563 scanning microscope (LSM710 META, Zeiss). High-resolution z-stack confocal images were
564 taken at 1 μm intervals and then merged using ImageJ software.

565 Immunohistochemistry was performed according to the following protocol. Free-floating sections
566 were rinsed in PBS and incubated with 10% normal donkey antiserum (NDS) and 0.2% Triton
567 X-100 in PBS for 60 min to reduce nonspecific staining and increase antibody penetration.
568 Sections were incubated overnight with primary antibodies diluted in PBS containing 1% NDS
569 and 0.2% Triton X-100. The following day, sections were washed in PBS, incubated with the

570 specific secondary antibodies conjugated to the fluorescent probes diluted in PBS for 2 h.
571 Sections were further washed in PBS, mounted, and coverslipped with Fluorsave mounting
572 medium (Millipore). The primary antibodies used for this study were as follows: rabbit polyclonal
573 anti-somatostatin-14 (1:500; Peninsula Laboratories), mouse monoclonal anti-NeuN (1:500;
574 Millipore; MAB377), goat anti-ChaT (1:500, Chemicon) and chicken polyclonal anti-GFP (1:500;
575 Aves Labs). DyLight488 donkey anti-chicken, Rhodamine Red-X donkey anti-rabbit, and Cy5
576 donkey anti-mouse conjugated secondary antibodies (1:250; Jackson ImmunoResearch) were
577 used to detect primary antibodies. Slides were observed under an AxioCam2 Zeiss fluorescent
578 microscope connected with AxioVision acquisition software or under a LSM510 Zeiss confocal
579 microscope with Zen software (Carl Zeiss). Images were acquired, exported in TIFF files, and
580 arranged to prepare final figures in Zen software (Carl Zeiss) and Adobe Photoshop (Adobe).

581 ***In vitro* electrophysiology**

582 Neonatal mice (P0-5) of either sex were anesthetized with isoflurane. The brainstem was
583 isolated from the pons to the rostral cervical spinal cord under cold ACSF containing (in mM):
584 124 NaCl, 3 KCl, 1.5 $CaCl_2$, 1 $MgSO_4$, 25 $NaHCO_3$, 0.5 NaH_2PO_4, and 30 D-glucose; a single
585 transverse slice (600μm) was cut on a vibratome (Leica VT1200S).

586 Slices were placed in a recording chamber with the rostral face of preBötC facing up and
587 continuously superfused with warmed ACSF (at 28-30°C) equilibrated with 95% O_2 and 5%
588 CO_2, and extracellular K^+ was increased to 9 mM to elevate preBötC excitability. Inspiratory-
589 related motor output was recorded from the hypoglossal nerve (XII) using a suction electrode
590 and a differential AC amplifier (AM systems), filtered at 2-4 kHz, integrated, and digitized at 10
591 kHz. Whole-cell recordings were made using a MultiClamp 700A (Molecular Devices), filtered at
592 2-4 kHz, and digitized at 10 kHz. Borosilicate glass recording electrodes (G150-4, Warner
593 Instruments) had tip resistances of 4-8 MΩ and were filled with intracellular solution containing
594 (in mM): 140 potassium gluconate, 10 HEPES, 5 NaCl, 1.1 EGTA, 2 Mg-ATP, and 0.1 $CaCl_2$
595 (~305 mOsm; pH 7.3). In two-photon imaging experiments, field potentials were recorded from

596 the contralateral preBötC, using an extracellular electrode and a differential AC amplifier (AM
597 systems), filtered at 2-4 kHz, integrated, and digitized at 10 kHz. Digitized data were analyzed
598 off-line using custom procedures written for IgorPro (Wavemetrics). Agonists were bath applied
599 at the specified concentrations while monitoring field potentials and XII output.

600 **Two-photon calcium imaging**

601 Intracellular Ca^{2+} was imaged using a multi-photon resonant scanner (3i) and a microscope
602 equipped with a water immersion 20x, 1.0 objective. Illumination was provided by a laser with a
603 power output of 1050 mW at 970 nm (Coherent Chameleon Ultra I). Identified preBötC neurons
604 were scanned at 10-39 Hz and fluorescence data were collected using 3i software and analyzed
605 using SlideBook, Image J and IgorPro. Regions of interest (ROIs) were manually detected and
606 Ca^{2+} transients were plotted as F/F_0, where F_0 is the average fluorescence intensity of all pixels
607 within a given ROI averaged over the entire time series.

608 **Statistical analysis**

609 *In vitro* data were analyzed using IgorPro (Wavemetrics) and GraphPad Prism (GraphPad
610 Software) was used for statistical analysis. Paired T-tests or Kruskal-Wallis one-way ANOVA,
611 adjusted for multiple comparisons, was used to calculate significance.

612 For *in vivo* experiments, data were recorded on a computer using LabChart 7 Pro (AD
613 Instruments) and analyzed using LabChart 7 Pro (ADInstruments), Excel, and Igor Pro
614 (Wavemetrics, Inc.) software. The flow signal was high-pass filtered (> 0.1 Hz) to eliminate DC
615 shifts and slow drifts, and was digitally integrated with a time constant of 0.05 s to calculate
616 breathing frequency, period, V_T, T_I and T_E during eupnea or sigh (Extended data Fig. 1d).
617 Breathing frequency is measured by the time interval between peaks. T_I was calculated by the
618 time interval from start to the maximum of the peak, T_E was calculated by the time interval from
619 the previous inspiratory peak to the onset of the next inspiratory burst and V_T was calculated
620 from the inspiratory peak. Due to high reproducibility of effects of photostimulation, V_T, T_I and T_E

during ectopic sighs were calculated as an average of 3-5 sighs, paired t-tests were used to determine statistical significance of changes before and after pharmacological injections or photostimulation. For statistical comparisons of more than two groups, repeated-measures (RM) ANOVAs were performed. For one-way RM ANOVAs, post hoc significance for pairwise-comparisons was analyzed using Holm-Sidak method. Significance was set at $p < 0.05$. Data are shown as mean ± SE.

Data availability

The data that support the findings of this study are available from the corresponding author, JLF, upon reasonable request.

Figures and Legends

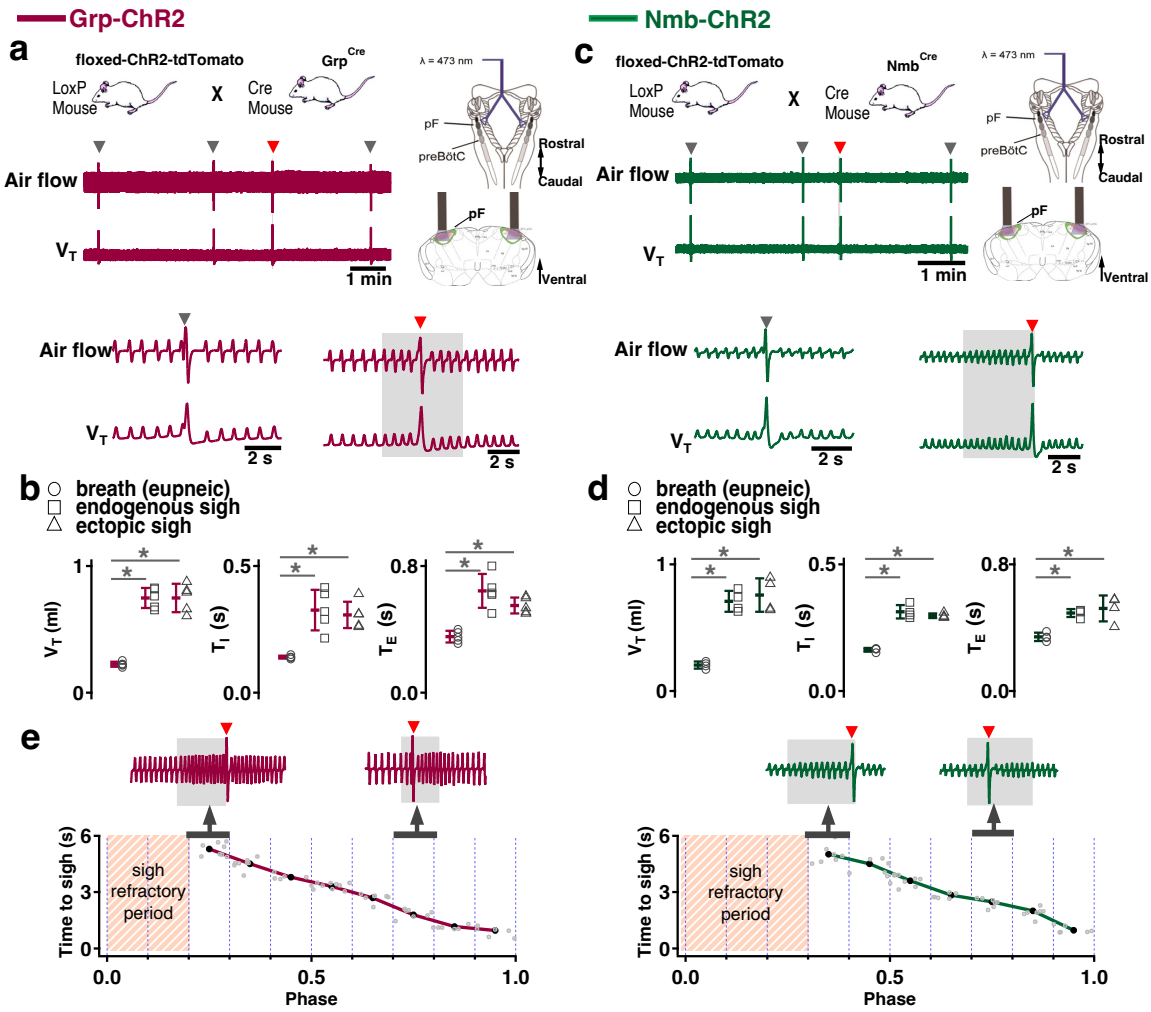

Fig. 1. Photostimulation of NMB and GRP pF neurons evoked sighing. **a**, Top: Breeding scheme to generate Grp-ChR2 mice. Schematic (right) depicting bilateral placement of optical cannula targeting pF. Middle and Bottom: Raw (middle) and expanded (bottom) traces show bilateral pF LPP (right gray box) in Grp-ChR2 mice elicits an ectopic sigh (red arrowhead) that appears similar to endogenous sighs (gray arrowheads). **b**, V_T (t_3 = 0.920, p = 0.393), T_I (t_3 = 1.811, p = 0.120), and T_E (t_3 = 0.277, p = 0.791) of ectopic sighs from pF Grp-ChR2

638 photostimulation were no different from endogenous sighs (n = 4 mice), but increased
639 compared to eupneic breaths (V_T: t_4 = 10.163, p = 5 x 10^{-5} T_I: t_3 = 6.224, p = 7 x 10^{-4}, T_E: t_4 =
640 7.152, p = 4 x 10^{-4}), indicative of augmented breaths with postsigh apneas. Statistical
641 significance was determined with a One Way RM ANOVA followed by All Pairwise Multiple
642 Comparison Procedures (Holm-Sidak method), V_T: $F_{2,9}$ = 63.194, p < 0.001; T_I: $F_{2,9}$ = 35.529,
643 p < 0.001; T_E: $F_{2,9}$ = 32.828, p < 0.001. **c**, Top: Breeding scheme to generate Nmb-ChR2 mice.
644 Schematic (right) depicting bilateral placement of optical cannula targeting pF. Middle and
645 Bottom: Raw (middle) and expanded (bottom) traces show bilateral pF LPP (right gray box) in
646 Nmb-ChR2 mice elicits ectopic sighs (red arrowhead) that appears similar to endogenous sighs
647 (gray arrowheads). **d**, V_T (t_3 = 2.436, p = 0.0508), T_I (t_3 = 0.603, p = 0.569), and T_E (t_3 = 0.308,
648 p = 0.768) of ectopic sighs from pF Nmb-ChR2 photostimulation were no different from
649 endogenous sighs (n = 4 mice), but increased compared to eupneic breaths (V_T: t_3 = 37.257,
650 p = 3 x 10^{-8}, T_I: t_3 = 6.697, p = 5 x 10^{-4}, T_E: t_3 = 7.074, p = 4 x 10^{-4}), indicative of augmented
651 breaths with postsigh apneas. Statistical significance was determined with a One Way RM
652 ANOVA followed by All Pairwise Multiple Comparison Procedures (Holm-Sidak method), V_T:
653 $F_{2,9}$ = 868.829, p < 0.001; T_I: $F_{2,9}$ = 27.450, p < 0.001; T_E: $F_{2,9}$ = 34.883, p < 0.001. **e**, Sigh
654 latency from laser onset was negatively correlated with sigh phase in Grp-ChR2 (r = -0.995,
655 p = 3 x 10^{-7}) and Nmb-ChR2 (r = -0.993, p = 8 x 10^{-6}) mice (Pearson Product Moment
656 Correlation). Top: Representative traces showing that latency between laser onset (gray box
657 indicates LPP) and ectopic sighs (red arrowheads) was longer when LPP was applied just after
658 the refractory period (pink diagonal stripes). Gray dots represent latency to ectopic sigh from
659 stimulation onset in each phase in Grp-ChR2 (n = 5 mice) and Nmb-ChR2 (n = 4 mice) mice,
660 solid lines join the average latency in each phase (black circle). No sighs were generated by
661 LPP in sigh phase 0.0–0.2 (34 ± 5 s from previous sigh, measured from 30 stimuli in 5 mice:
662 basal sigh rate 21 ± 3/hour, range 17–25; intersigh interval 172 ± 25 s) in Grp-ChR2 and in
663 phase 0.0–0.3 (58 ± 20 s from previous sigh, measured from 48 stimulus in 4 mice: basal sigh
664 rate 20 ± 7/hour, range 13-27; intersigh interval 193 ± 65 s) in Nmb-ChR2 mice. Data are shown

as mean ± SE. Asterisks indicate post-hoc multiple comparison test results or paired t-test results: *, significance with $p < 0.05$.

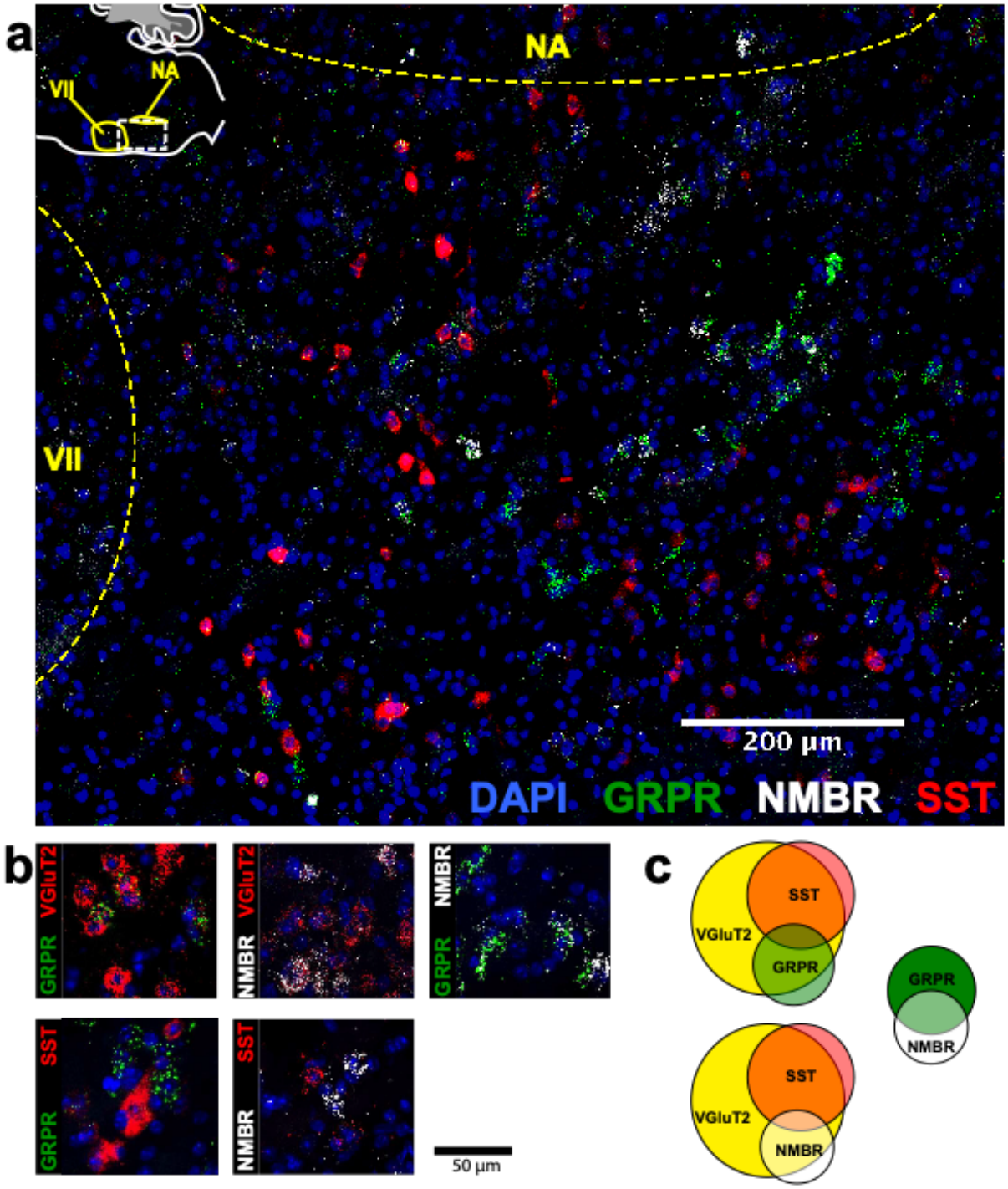

668 **Fig. 2. NMBR and GRPR neurons in preBötC are mainly glutamatergic, but mostly not**
669 **somatostatinergic. a**, Sagittal section of medulla with NMBR (white), GRPR (green) and SST
670 (red) RNAscope signals as well as DAPI (blue) at the level of preBötC; inset top left: location of
671 image (line box) in mouse medulla. **b**, Examples of colocalization between relevant markers in
672 high magnification confocal images (100 x 100 μm) of tissues processed with RNAscope.
673 **c**, Venn diagrams representing relative number of preBötC neurons expressing relevant
674 markers and their overlap, scaled according to total Vglut2 count (n = 3 sections for each
675 colocalization pair). VII: facial nucleus. NA: nucleus ambiguous. There were 22.6 ± 2.3 $GRPR^+$
676 neurons and 14.6 ± 1.4 $NMBR^+$ neurons in each transverse section; 25/45 $NMBR^+$ neurons
677 coexpressed GRPR; 25/77 $GRPR^+$ neurons coexpressed NMBR. Majority of both $NMBR^+$ and
678 $GRPR^+$ co-expressed VgluT2 (47/55 and 63/76, respectively), but not SST (6/46 and 5/54,
679 respectively).
680

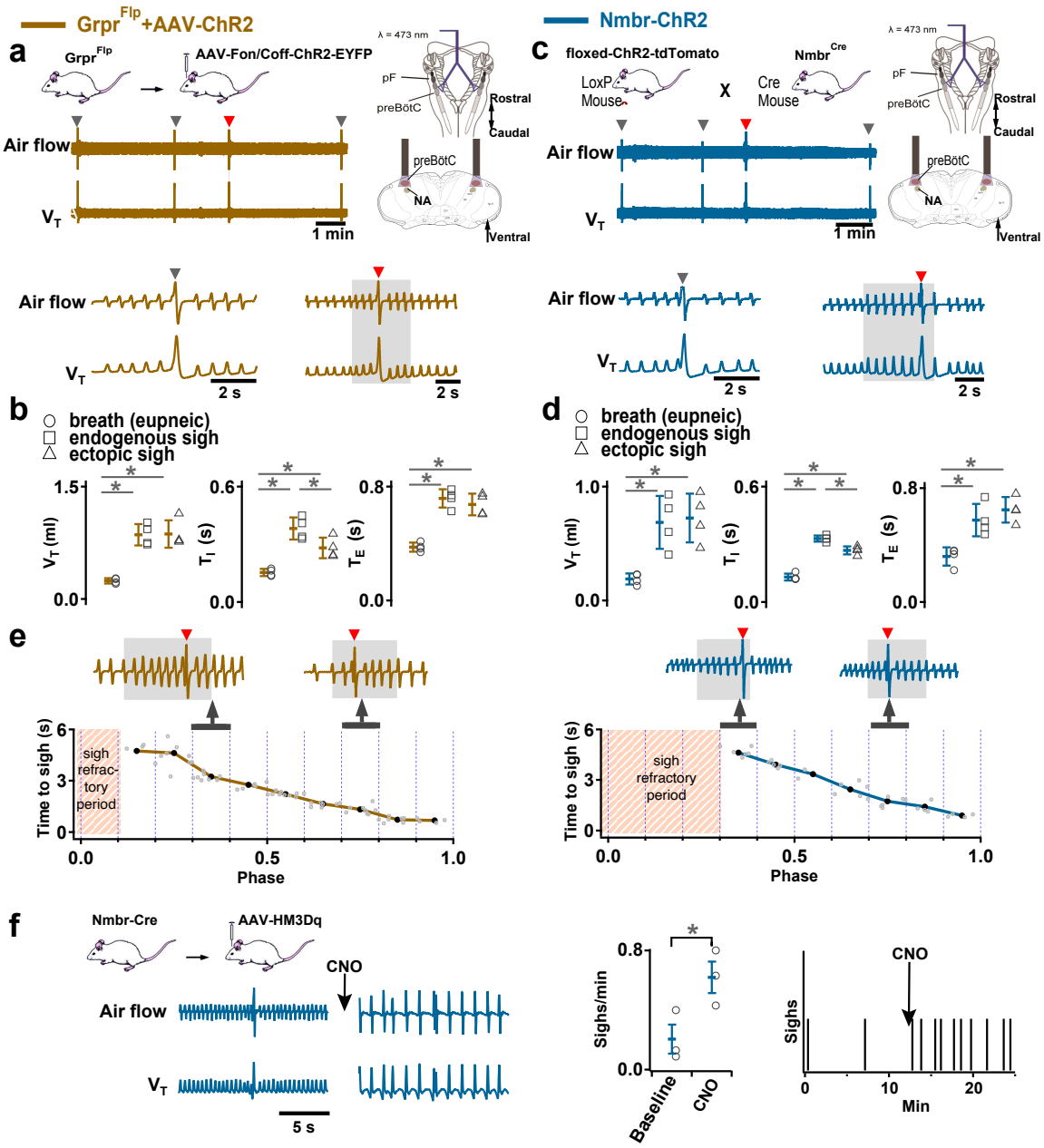

681

682 **Fig. 3. Excitation of preBötC GRPR or NMBR neurons induced sighs.** (a-e)
683 Photostimulation of preBötC GRPR (brown) or NMBR (blue) neurons evoked sighs. **a**, Top:
684 Schematic of genetic strategy to target preBötC GRPR neurons. Schematic (right) depicting
685 bilateral placement of optical cannula targeting preBötC. Middle and Bottom: Raw (middle) and
686 expanded (bottom) traces show bilateral LPP (gray box) of preBötC GRPR neurons could elicit
687 an ectopic sigh (red arrowhead). Gray arrowheads indicate endogenous sighs. **b**, Photo-

688 stimulation of preBötC GRPR induced ectopic sighs with similar V_T and T_E as endogenous
689 sighs, but slightly lower T_I (V_T: $t_3 = 0.233$, $p = 0.824$; T_E: $t_3 = 0.249$, $p = 0.812$; T_I: $t_3 = 3.267$, $p <$
690 0.05). V_T, T_E and T_I of ectopic sighs were significantly greater than those of eupneic breaths (V_T:
691 $t_3 = 6.889$, $p = 5 \times 10^{-4}$; T_I: $t_3 = 3.183$, $p = 0.019$; T_E: $t_3 = 8.675$, $p = 3 \times 10^{-4}$). Statistical
692 significance was determined with a One Way RM ANOVA followed by All Pairwise Multiple
693 Comparison Procedures (Holm-Sidak method), V_T: $F_{2,9} = 32.744$, $p < 0.001$; T_I: $F_{2,9} = 16.530$,
694 $p < 0.001$; T_E: $F_{2,9} = 48.771$, $p < 0.001$. **c**, Top: Targeting scheme to generate Nmbr-ChR2 mice.
695 Schematic (right) depicting bilateral placement of optical cannula targeting preBötC. Middle and
696 Bottom: Raw (middle) and expanded (bottom) show bilateral LPP (gray box) of preBötC NMBR
697 neurons could elicit an ectopic sigh (red arrowhead). Gray arrowheads indicate endogenous
698 sighs. **d**, Photostimulation of preBötC NMBR neurons induced ectopic sighs with similar V_T and
699 T_E as endogenous sighs, but slightly lower T_I (V_T: $t_3 = 0.820$, $p = 0.444$; T_E: $t_3 = 0.976$, $p = 0.367$;
700 T_I: $t_3 = 3.175$, $p = 0.0192$). V_T, T_E and T_I of ectopic sighs were significantly greater than those of
701 eupneic breaths (V_T: $t_3 = 9.756$, $p = 7 \times 10^{-5}$; T_I: $t_3 = 7.685$, $p = 3 \times 10^{-4}$; T_E: $t_3 = 7.326$, $p = 3 \times 10^{-}$
702 ^{4}). Statistical significance was determined with a One Way RM ANOVA followed by All Pairwise
703 Multiple Comparison Procedures (Holm-Sidak method), V_T: $F_{2,9} = 58.564$, $p < 0.001$; T_I:
704 $F_{2,9} = 62.362$, $p < 0.001$; T_E: $F_{2,9} = 31.646$, $p < 0.001$. **e**, Latency from laser onset was negatively
705 correlated with phase in $Grpr^{Flp}$ ($r = -0.980$, $p = 4 \times 10^{-6}$) and Nmbr-ChR2 ($r = -0.994$, $p = 6 \times 10^{-}$
706 ^{6}) mice (Pearson Product Moment Correlation). Representative traces showing latency between
707 laser onset (gray box indicates LPP) and ectopic sighs (red arrowheads) when LPP was applied
708 in medial (0.4) and late (0.8) phase. Gray dots represent latency to ectopic sigh from stimulation
709 onset in each phase in $Grpr^{Flp}$ (n = 5 mice) and Nmbr-ChR2 (n = 4 mice) mice, solid lines join
710 the average latency in each phase (black circle). No sighs were generated by LPP in phase
711 0.0–0.1 (23 ± 4 s from previous sigh, measured from 55 stimulus in 5 mice: basal sigh rate
712 16 ± 2 h/hour, range 12–19; intersigh interval 230 ± 41 s) in $Grpr^{Flp}$ and in phase 0.0–0.3 (61 ±
713 21 s from previous sigh, measured from 50 stimulus in 4 mice: basal sigh rate 19 ± 6 h/hour,
714 range 12-25; intersigh interval 203 ± 70 s) in Nmbr-ChR2 mice. **f**, Chemogenetic activation of
715 preBötC NMBR neurons induced sighs. Left top: schematic diagram of genetic strategy to

selectively express DREADD receptor hM3Dq on preBötC NMBR neurons. Left bottom: representative traces of airflow and V_T before and after application of CNO to brainstem surface. Middle: Activation of hM3Dq receptors expressed on NMBR neurons with CNO significantly increases sigh rate (paired two-tailed t-test, n = 3 mice: $t_2 = 5.94$, $p = 0.03$). Right: Trace from a representative mouse illustrating incidence of sighs before and after CNO application. Data are shown as mean ± SE. Asterisks indicate post-hoc multiple comparison test results or paired t-test results: *, significance with $p < 0.05$.

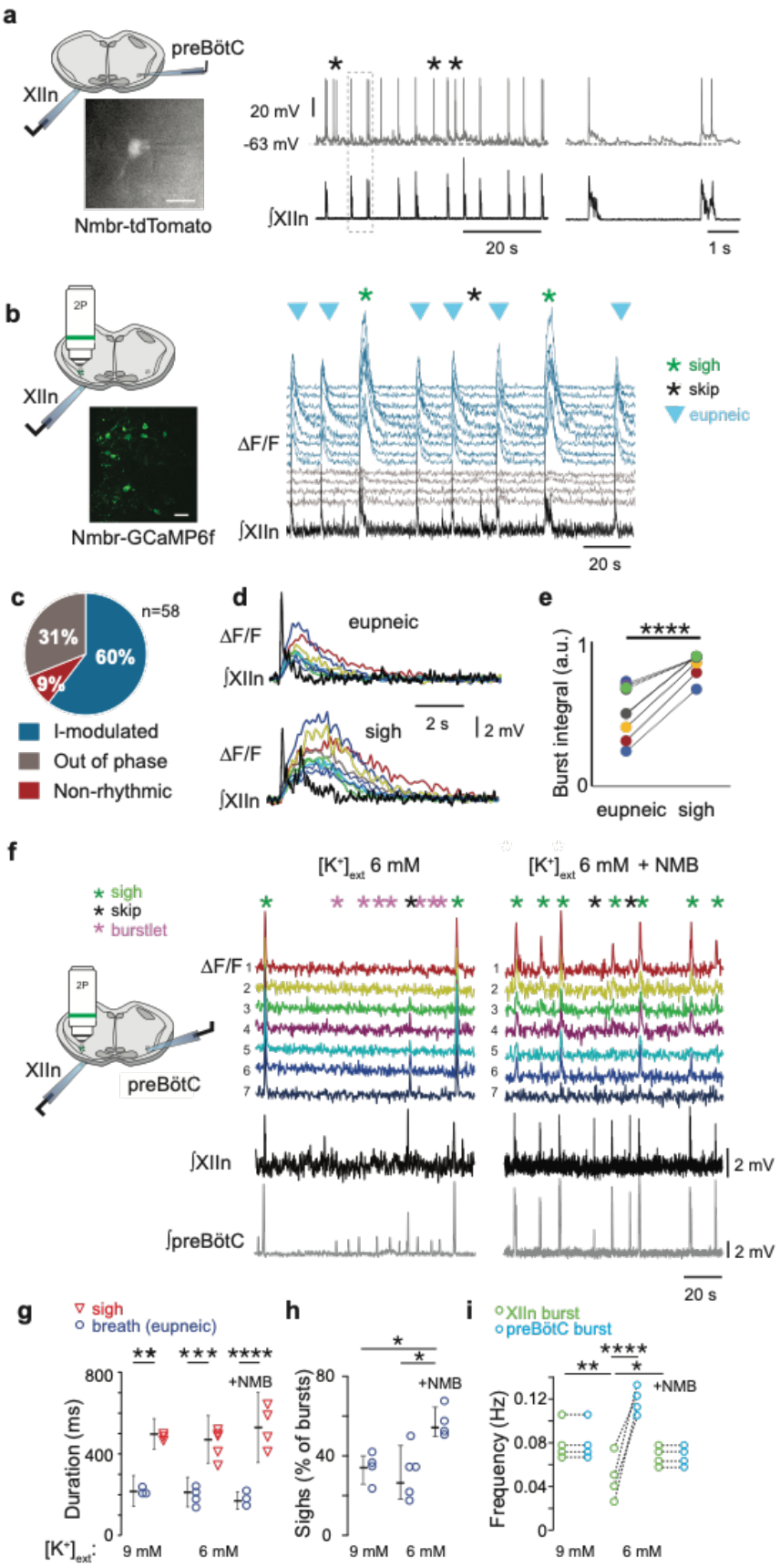
a
preBötC
XIIn
Nmbr-tdTomato
20 mV
-63 mV
∫XIIn
20 s
1 s
b
2P
XIIn
Nmbr-GCaMP6f
ΔF/F
∫XIIn
20 s
sigh
skip
eupneic
c
n=58
31%
60%
9%
I-modulated
Out of phase
Non-rhythmic
d
eupneic
ΔF/F
∫XIIn
sigh
2 s
2 mV
e
****
Burst integral (a.u.)
eupneic
sigh
f
[K+]ext 6 mM
[K+]ext 6 mM + NMB
sigh
skip
burstlet
ΔF/F
XIIn
preBötC
∫XIIn
∫preBötC
2 mV
20 s
g
sigh
breath (eupneic)
Duration (ms)
+NMB
[K+]ext:
9 mM
6 mM
h
Sighs (% of bursts)
+NMB
9 mM
6 mM
i
XIIn burst
preBötC burst
Frequency (Hz)
+NMB
9 mM
6 mM

725 **Fig. 4. NMBR neurons in preBötC were rhythmically active *in vitro* and NMB converted**
726 **inspiratory burstlets into sighs and bursts. a**, Left: schematic of slice preparation with
727 photograph of patched Nmbr-tdTomato preBötC neuron. Scale bar: 50 µm. Right: Whole cell
728 current clamp recording from inspiratory-modulated preBötC NMBR neuron (top trace_ that
729 generated action potentials (APs) during each XII burst (bottom trace). Not every cluster of APs
730 (*) is associated with a burst, but each burst was associated with one or more Aps. Far right:
731 Two bursts shown at expanded timescale. **b**, Left: schematic of slice preparation in 2P
732 experiment with image of GCaMP6f-expressing preBötC neurons. Scale bar 50 µm. Right:
733 Representative Ca^{2+} signal of neighboring preBötC NMBR neurons was correlated with XIIn
734 bursts (9 mM $[K^+]_{ext}$). Large amplitude XIIn bursts represent sighs (green asterisks), XIIn bursts
735 not associated with Ca^{2+} signal indicated with black asterisks. **c**, Percentage of rhythmically
736 active (I-modulated), non-rhythmic and out of phase preBötC NMBR neurons in preBötC. **d**,
737 Ca^{2+} transients in individual neurons were significantly larger during sighs than during eupneic
738 bursts (paired two-tailed t-test: $t_8 = 7.14$, $p < 0.001$). **e**, Intervals of sighs were significantly
739 greater during sighs compared to eupneic burst (same color-coded neurons as in d). **f**, Left:
740 schematic of slice preparation and configuration. Right: Simultaneous Ca2+ signal from NMBR
741 neurons (n = 7), preBötC field recording, and XIIn activity in control conditions ($[K^+]_{ext}$ = 6 mM)
742 and after addition of NMB (30 nM). Burstlets (red asterisks) are seen in control but not with
743 NMB. **g**, Quantification of duration of eupneic and sigh bursts in 9mM $[K^+]_{ext}$ and 6mM $[K^+]_{ext}$ with
744 or without NMB. Differences in duration between eupneic bursts in different conditions, and
745 between sighs in different conditions were not significant (repeated measures ANOVA,
746 $F_{5,19} = 20.1$, $p < 0.001$; asterisks indicate significance from Tukey post-hoc tests). **h**, Percentage
747 of bursts that were sighs during 5 min was significantly higher in 6 mM $[K^+]_{ext}$ + NMB than other
748 conditions (repeated measures ANOVA, $F_{2,9} = 7.18$, $p = 0.018$). **i**, Comparisons between XIIn
749 burst frequency and preBötC burst frequency in in 9mM $[K^+]_{ext}$ and 6mM $[K^+]_{ext}$ with or without
750 NMB. XIIn and preBötC burst frequency were similar in 9mM $[K^+]_{ext}$ and 6mM $[K^+]_{ext}$ + NMB, and
751 both conditions differ from 6mM $[K^+]_{ext}$ alone. There is an increase in preBötC burst frequency in
752 6mM [K+]ext due to the burstlets (shown in a), (repeated measures ANOVA, $F_{5,23} = 11.57$,

753 $p < 0.001$). Data are shown as mean ± SE. Asterisks indicate significance from Tukey post-hoc

754 tests or paired t-tests: *, significance with $p < 0.05$; **, significance with $p < 0.01$; ***,

755 significance with $p < 0.001$.

756

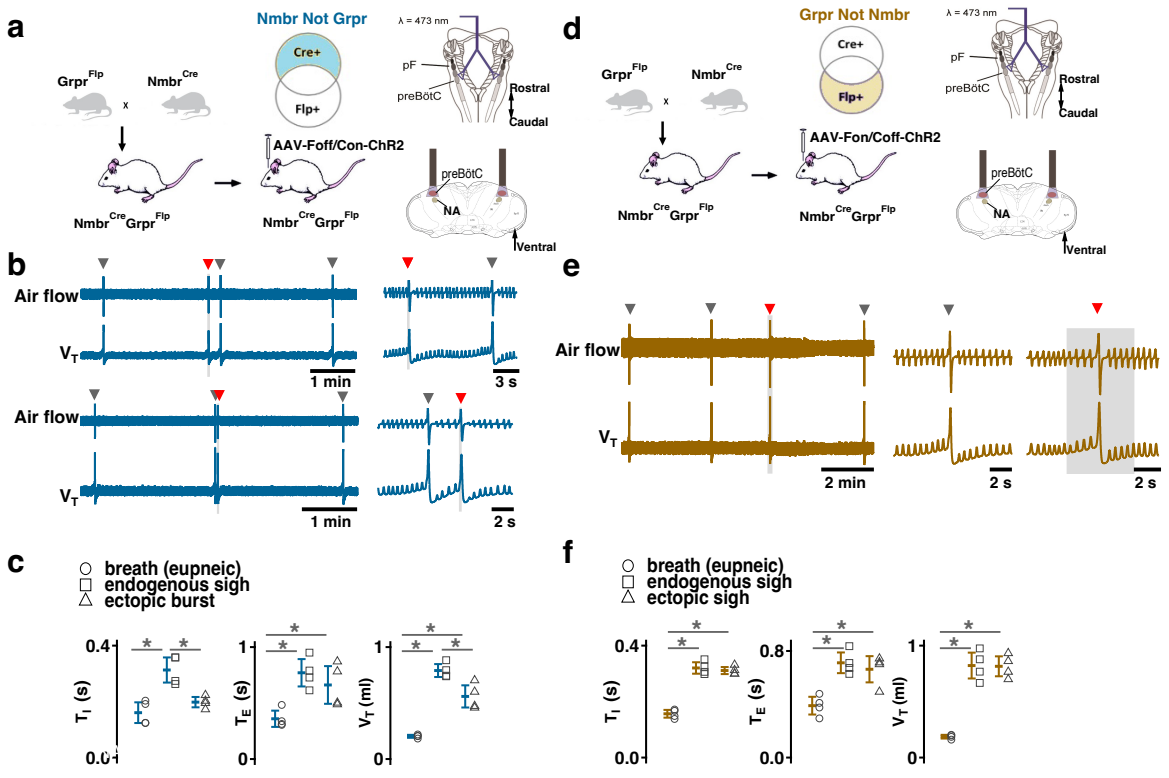

Fig. 5. Effects of activating preBötC NMBR-only or GRPR-only neurons on the generation of sighs. (a-c) Effects of activating preBötC NMBR-only neurons on sigh generation. **a,** Left: Schematic of the intersectional genetic strategy to target preBötC NMBR-only neurons. Right: Schematic depicting bilateral placement of optical cannula targeting preBötC. **b,** Top: Raw (left) and expanded (right) traces show that preBötC SPP (gray box) of NMBR-only neurons induced an ectopic burst (red arrowhead) which did not reset the sigh rhythm. Bottom: preBötC SPP of NMBR-only neurons induced an ectopic burst (red arrowhead) in a sigh refractory period. Gray arrowheads indicate endogenous sighs. **c,** V_T of ectopic bursts evoked by NMBR-only photostimulation was smaller than that of endogenous sighs (n = 4 mice, t_3 = 4.278, p = 0.005), but larger than of eupneic breaths (t_3 = 6.588, p = 6 x 10^{-4}); T_E of evoked ectopic bursts was no different from endogenous sighs (t_3 = 1.882, p = 0.109) , but higher than of eupneic breaths (t_3 = 5.203, p = 0.002); T_I of evoked ectopic bursts was shorter than that of endogenous sighs (t_3 = 3.917, p = 0.008). Statistical significance was determined with a One Way RM ANOVA followed by All Pairwise Multiple Comparison Procedures (Holm-Sidak method), V_T:

773 $F_{2,9}$ = 59.922, p < 0.001; T_I: $F_{2,9}$ = 25.206, p < 0.001; T_E: $F_{2,9}$ = 26.939, p < 0.001. (d-f) Effects of
774 activating preBötC GRPR-only neurons on sigh generation. **d,** Left: Schematic of the
775 intersectional genetic strategy to target preBötC GRPR-only neurons. Right: Schematic
776 depicting bilateral placement of optical cannula targeting preBötC. **e,** preBötC LPP of GRPR-
777 only neurons in late phase elicited ectopic sighs and reset the sigh rhythm. Raw (left) and
778 expanded (middle and right) show bilateral LPP (gray box) of preBötC GRPR-only neurons
779 elicited an ectopic sigh (red arrowhead). Gray arrowheads indicate endogenous sighs. **f,** V_T
780 (t_3 = 0.152, p = 0.884), T_I (t_3 = 1.843, p = 0.115) and T_E (t_3 = 1.619, p = 0.157), of ectopic sighs
781 were no different from endogenous sighs (n = 4 mice), but increased compared to eupneic
782 breaths (V_T:, t_3 = 12.855, p = 10^{-5}; T_I: t_3 = 30.235, p = 9 x 10^{-8}; T_E: t_3 = 9.007, p = 4 x 10^{-5}),
783 indicative of augmented breaths with postsigh apneas. Statistical significance was determined
784 with a One Way RM ANOVA followed by All Pairwise Multiple Comparison Procedures (Holm-
785 Sidak method), V_T: $F_{2,9}$ = 111.488, p < 0.001; T_I: $F_{2,9}$ = 648.855, p < 0.001; T_E: $F_{2,9}$ = 65.544, p <
786 0.001. Data are shown as mean ± SE. Asterisks indicate post-hoc multiple comparison test or
787 paired t-test results: *, significance with p <0 .05.
788

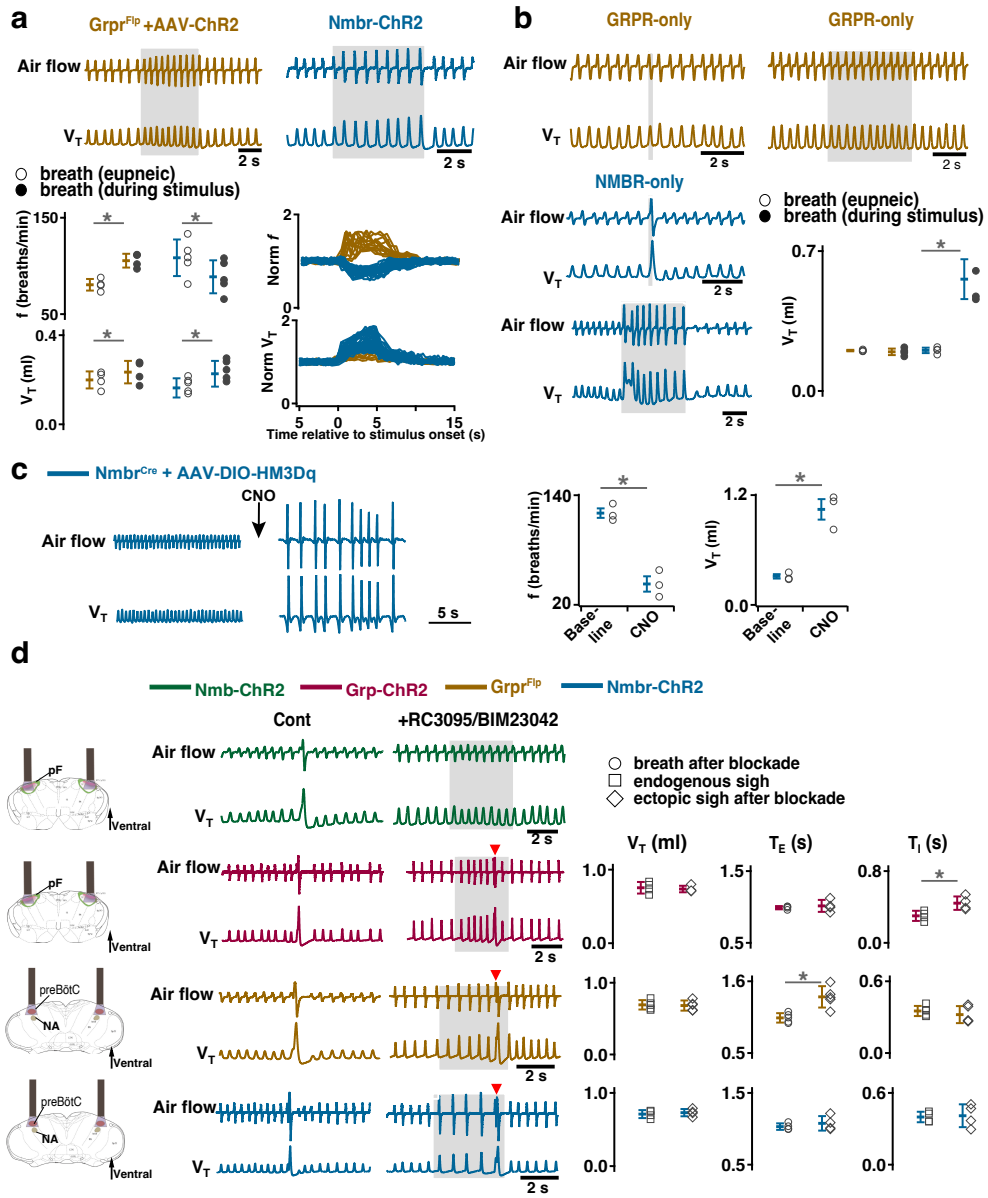

Fig. 6. Distinct roles of preBötC GRPR and NMBR neurons on inspiratory burst amplitude and sigh generation after receptor blockade. a, Photostimulation of preBötC GRPR (brown) and NMBR (blue) neurons perturbs breathing frequency and inspiratory burst amplitude. Top: representative traces recorded during sigh refractory period show effects of bilateral preBötC LPP of preBötC GRPR (brown) or NMBR (blue) neurons on eupneic breathing f and V_T. Bottom: V_T and *f* of eupneic breaths and during photostimulation. (paired t-tests, Grpr^{Flp} + AAV-ChR2, n = 4 mice, *f*: t_3 = -8.13801, p = 4 x 10^{-3}; V_T: t_3 = -5.035, p = 0.015; Nmbr-ChR2, n = 5 mice, *f*:

797 t_4 = 7.33379, p = 2 x 10^{-3}, V_T: t_4 = -5.875, p = 4 x 10^{-3}). Normalized (norm) V_T and *f* traces
798 relative to stimulus onset measured prestimulation, during stimulation and poststimulation. **b,**
799 Distinct effects of activating preBötC GRPR-only (brown) and NMBR-only (blue) neurons on
800 inspiratory burst amplitude. Top and bottom (left): representative traces show the effects of
801 bilateral preBötC SPP and LPP of preBötC GRPR-only (brown) or NMBR-only (blue) neurons
802 on breathing V_T. Bottom (right): V_T of eupneic breaths and during SPP stimulation. Increase in
803 V_T in response to bilateral preBötC SPP of preBötC GRPR-only (brown) or NMBR-only (blue)
804 neurons (paired t-tests, GRPR-only, n = 4 mice: t_3 = 0.746, p = 0.510; NMBR-only, n = 4 mice:
805 t_3 = -6.886, p = 6 x 10^{-3}). **c,** Activation of hM3Dq receptors expressed on NMBR neurons with
806 CNO significantly increased breathing amplitude and decreased *f* (paired two-tailed t-tests,
807 n = 3 mice, *f*: t_2 = 5.71, p = 0.03; V_T: t_2 = 5.47, p = 0.03). **d,** Sighs can be induced after GRPR
808 and NMBR inhibition. Left: schematic depicting bilateral placement of optical cannula targeting
809 pF or preBötC. Middle: representative traces showing LPP of pF GRP neurons, or preBötC
810 GRPR and NMBR neurons elicited ectopic sighs (doublet, red arrowhead), but not of pF NMB
811 neurons, in the presence of GRPR antagonist RC3095 and NMBR antagonist BIM23042. Right:
812 V_T of doublets induced by pF LPP of GRP neurons was not significantly different from that of
813 endogenous sighs (n = 4 mice; t_3 = 0.724, p = 0.522); T_I increased compared to endogenous
814 sighs (t_3 = -7.493, p = 5 x 10^{-3}), T_E of the following respiratory cycle was unaffected (t_3 = -0.472,
815 p = 0.669). V_T and T_I of the doublets elicited by preBötC LPP of GRPR (n = 5 mice, V_T:
816 t_4 = 0.199, p = 0.852; T_I: t_4 = 0.912, p = 0.413) or NMBR (n = 4 mice, V_T: t_3 = -0.845, p = 0.460;
817 T_I: t_3 = -0.376, p = 0.732) neurons after blockade of both receptors were not different from
818 spontaneous sighs. T_E immediately following doublet increased in $Grpr^{Flp}$ (n = 5 mice,
819 t_4 = -3.144, p = 0.035), but not lengthened in Nmbr-ChR2 mice (n = 4 mice, t_3 = -0.801,
820 p = 0.482). Data are shown as mean ± SE. Asterisks indicate post-hoc multiple comparison test
821 or paired t-test results: *, significance with p < 0.05.

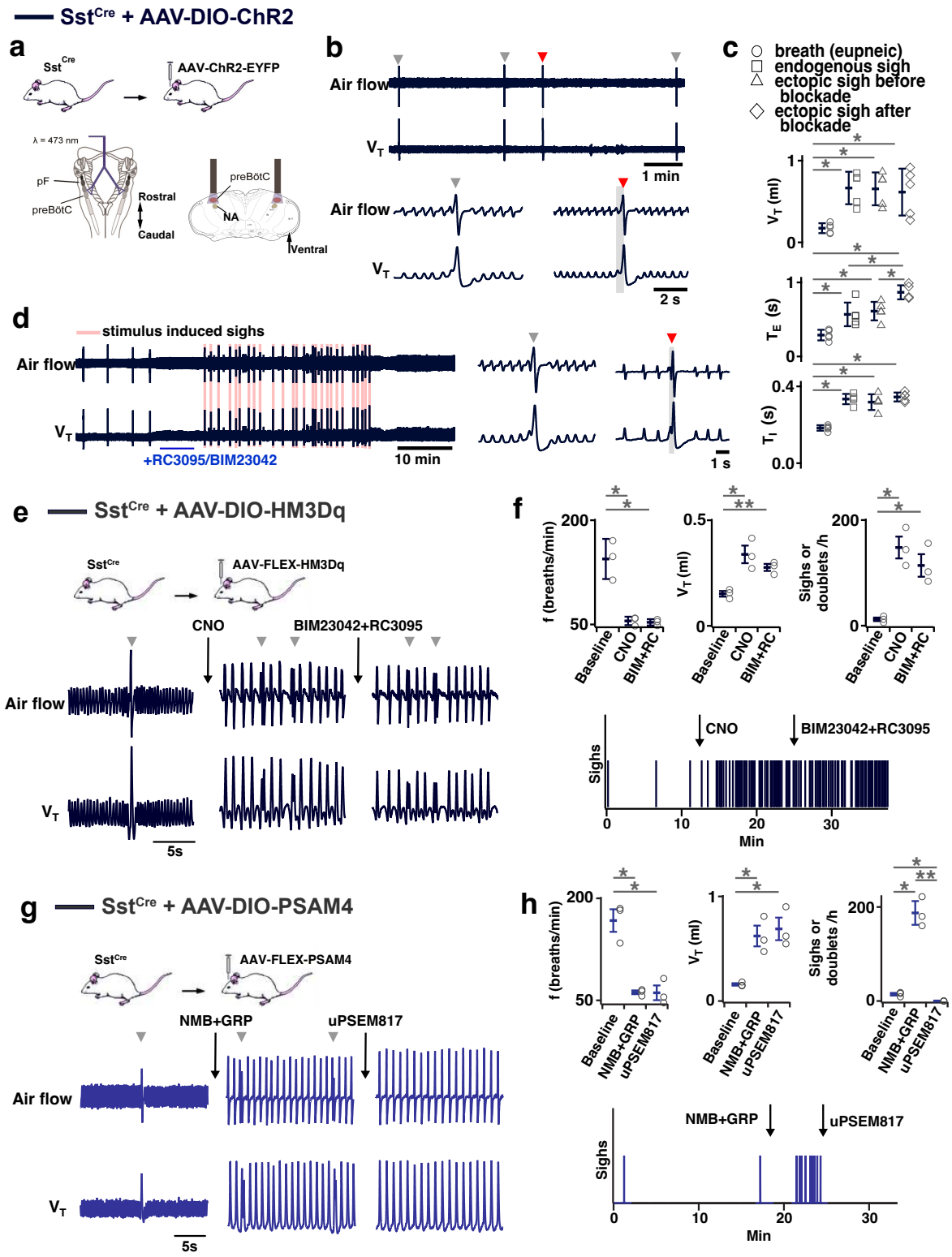

822

823 **Fig. 7. Effects of activation or inhibition of preBötC SST neurons on sigh generation**. (a-d)

824 Optogenetic activation of SST neurons generates sighs after blockade of NMBRs and GRPRs.

825 **a,** Top: Schematic of the genetic strategy to target preBötC SST neurons. Bottom: Schematic
826 depicting bilateral placement of optical cannula targeting preBötC. **b,** Ectopic sigh (red
827 arrowhead) elicited by bilateral SPP (gray box) of preBötC SST neurons. **c,** V_T (t_4 = 0.176,
828 p = 0.863), T_I (t_4 = 1.355, p = 0.200), T_E (t_4 = 0.734, p = 0.477) of ectopic sighs before blockade
829 or V_T (t_4 = 0.856, p = 0.409), T_I (t_4 = 0.894, p = 0.389) of ectopic sighs after blockade of NMBR
830 and GRPR were no different from endogenous sighs (n = 5 mice). T_E of ectopic sighs elicited
831 after blockade was longer than that of endogenous sighs (t_4 = 4.960, p = 3 x 10^{-4}). V_T, T_I, and T_E
832 of ectopic sighs before; V_T: t_4 = 7.925, p = 4 x 10^{-6}; T_I: t_4 = 11.194, p = 10^{-7}; T_E: t_4 = 5.405,
833 p = 10^{-4}) or after (V_T: t_4 = 7.245, p = 10^{-5}; T_I: t_4 = 13.442, p = 10^{-8}; T_E: t_4 = 9.631, p = 5 x 10^{-7})
834 blockade were increased compared with eupneic breaths (n = 5 mice), indicative of augmented
835 breaths with postsigh apneas. Statistical significance was determined with a One Way RM
836 ANOVA followed by All Pairwise Multiple Comparison Procedures (Holm-Sidak method), V_T:
837 $F_{3,16}$ = 30.357, p < 0.001; T_I: $F_{3,16}$ = 78.526, p < 0.001; T_E: $F_{3,16}$ = 31.134, p < 0.001. **d,** SPP
838 elicits sighs in the presence of GRPR antagonist RC3095 and NMBR antagonist BIM23042. (e-
839 f) Chemogenetic activation of SST neurons generated sighs after blockade of NMBRs and
840 GRPRs. **e,** Top: schematic diagram of genetic strategy to selectively express DREADD receptor
841 hM3Dq on preBötC SST neurons. Bottom: representative trace of airflow and V_T during
842 baseline, after application of CNO, and after microinjection of RC3095 and BIM23042. **f,** Top:
843 Activation of hM3Dq receptors expressed on preBötC SST^+ neurons significantly decreased
844 breathing *f*, increases V_T, and elevated sigh frequency; subsequent BIM23042 and RC3095
845 (B+R) microinjection into preBötC did not significantly affect breathing *f*, V_T, nor sigh rate
846 induced by CNO application (repeated measures ANOVA, n = 3 mice; *f*: $F_{2,4}$ = 28.3, p = 0.004;
847 V_T: $F_{2,4}$ = 25.7, p = 0.005; sigh rate: $F_{2,4}$ = 26.1, p = 0.005). Bottom: representative trace
848 depicting sighs during baseline, after application of CNO and after microinjection of NMBR and
849 GRPR antagonists RC3095 and BIM23042. **g,** Top: schematic diagram of genetic strategy to
850 selectively express ultrapotent inhibitory DREADD receptor PSAM4-GlyR on preBötC SST^+
851 neurons. Bottom: representative trace of airflow and V_T during baseline, after preBötC
852 microinjection of peptides NMB and GRP (250 μM each, 50nl/side), and application of

uPSEM817 (10mM, 30μl applied to brainstem surface). **h,** Top: Microinjection of peptides NMB and GRP into preBötC significantly decreased breathing *f,* increased V_T, and elevated sigh frequency; subsequent inhibition of SST+ preBötC neurons selectively eliminated any sighs, but preserves decreased *f* and V_T (repeated measures ANOVA, n = 3 mice; f: $F_{2,4} = 55.8$, $p = 0.001$; V_T: $F_{2,4} = 19.0$, $p = 0.009$; sigh rate: $F_{2,4} = 83.8$, $p < 0.001$). Bottom: representative trace depicting sighs during baseline, after bilateral preBötC microinjection of NMB and GRP and after application of PSAM4-GlyR ligand uPSEM817 to the brainstem surface. Data are shown as mean ± SE. Asterisks indicate post-hoc multiple comparison test or paired t-test results: *, significance with $p < 0.05$; **, significance with $p < 0.01$.

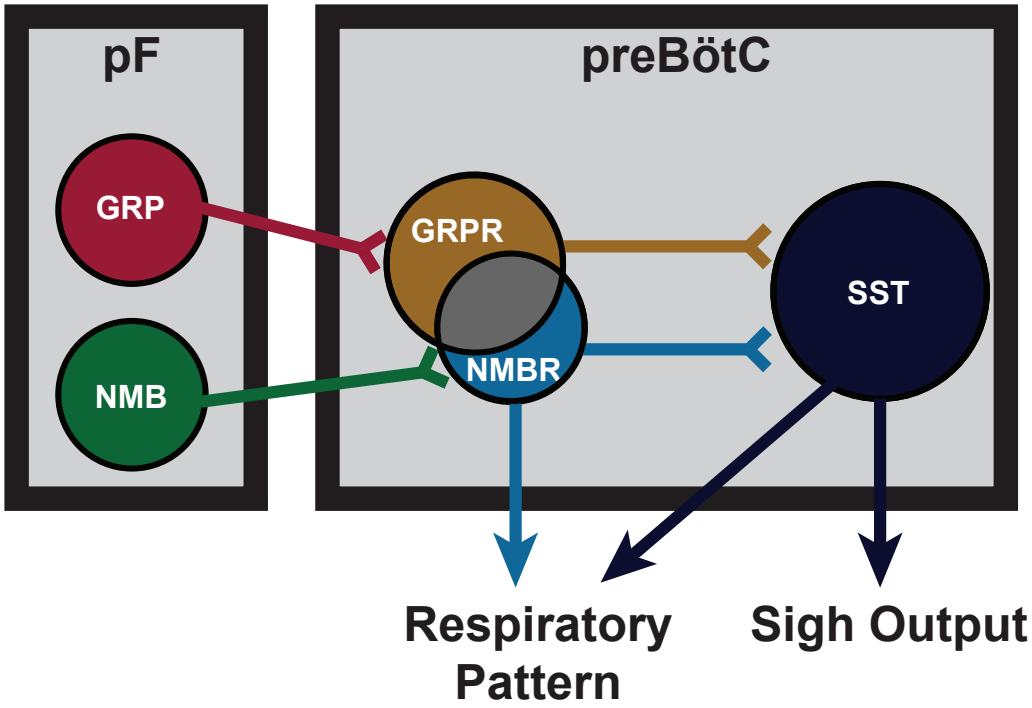

863

864 **Fig. 8. Proposed model of sigh generating pF-preBötC microcircuit.** NMB and GRP
865 neurons in pF project to preBötC neurons expressing cognate receptors NMBR and GRPR.
866 NMBR and GRPR preBötC neurons mediate sigh output via connections to downstream SST
867 preBötC neurons, but also directly contribute to the pattern of eupneic breathing.

868

Extended Data

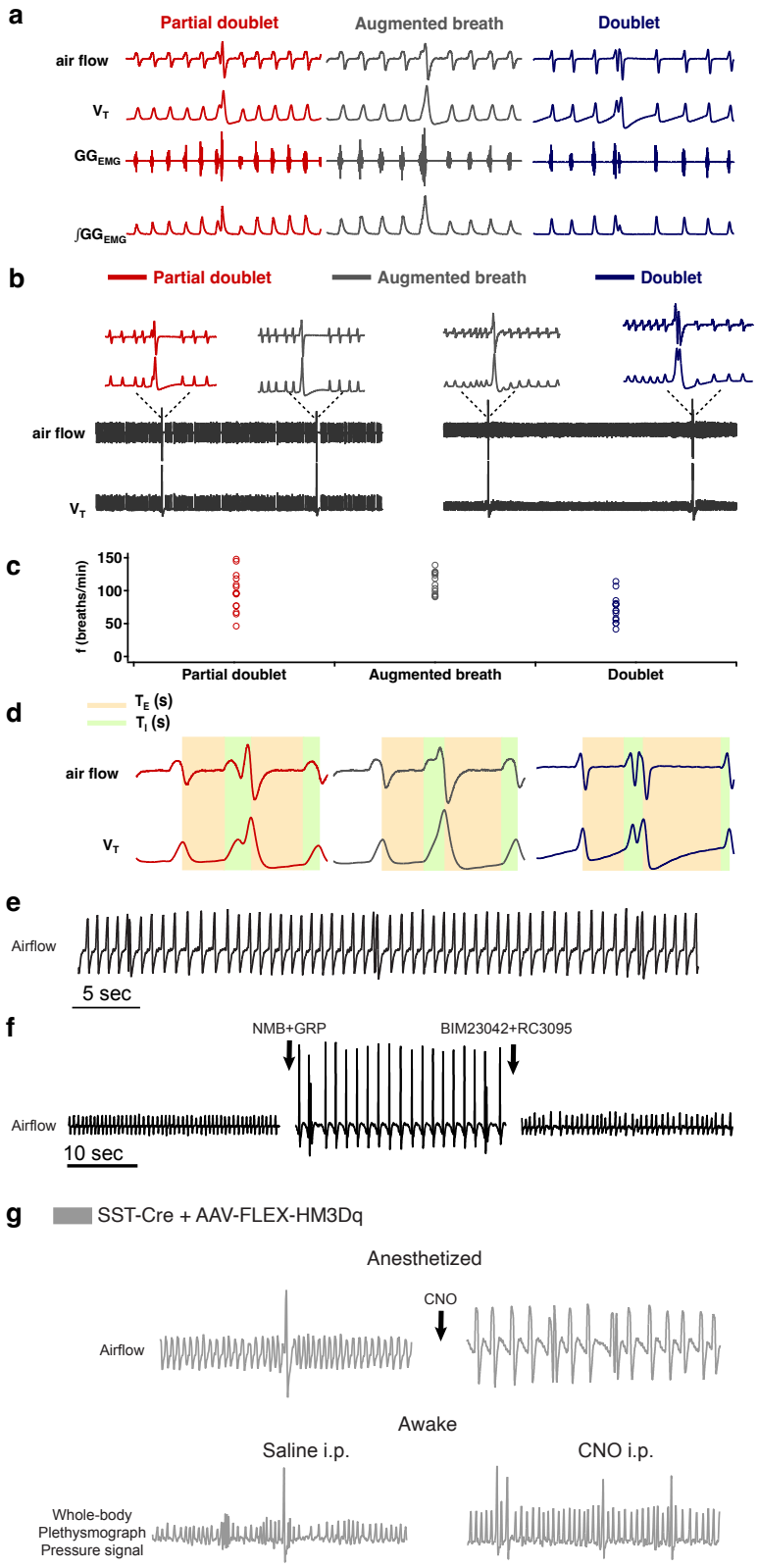

871 **Extended data Fig. 1. a,** Three types of sighs observed in adult mice *in vivo*. A sigh is a
872 spontaneous inspiratory effort that results in significantly increased inspiratory tidal volume,
873 typically two to five times compared to normal breaths. Under anesthesia in mice, sighs *in vivo*
874 can take multiple shapes. The most common shape is partial doublet, a biphasic double-sized
875 breath with an initial phase that is identical to a normal breath (eupnea) and a later high-
876 amplitude inspiration, coincident with a biphasic genioglossus$_{EMG}$ (GG$_{EMG}$) event (left). An *in vivo*
877 sigh in mice can also present as one large breath, a monophasic augmented inspiration that has
878 two to five times the volume of a normal breath, coincident with a monophasic GG$_{EMG}$ event
879 (middle); or a double-peaked breath (doublets) with the first breath immediately followed by a
880 similar amplitude second breath (right). **b**, Raw and expanded traces show three types of shape
881 observed in one mouse. **c**, Sigh shapes are related to basal breathing frequency (45
882 spontaneous sighs from 3 mice). Different sigh shapes represent a continuum from "augmented
883 breath" on one side of the spectrum to "doublet" on the other. Exact shape appears to be related
884 to basal breathing frequency, with augmented breaths and occasional partial doublets exhibited
885 during conditions with high basal respiratory rate/low amplitude; while doublets and partial
886 doublets occur mostly with low basal respiratory rate/high amplitude. The latter is similar to
887 conditions of vagotomy and *in vitro*, where breathing *f* is substantially reduced, and during which
888 sighs often appeared as doublets. **d**, Measurement of respiratory parameters of eupneic breath
889 and three types of sighs. **e,** Sighs exhibiting a doublet shape occur periodically at a frequency
890 significantly lower than normal eupneic breaths after NMB and GRP microinjection into preBötC
891 in ketamine/xylazine anesthetized mice. **f,** Doublets are not artefacts resulting from any damage
892 to preBötC, since doublet-shaped sighs induced by microinjection of NMB and GRP were
893 blocked by subsequent preBötC microinjection of NMBR and GRPR antagonists BIM23042 and
894 RC3095. **g,** Chemogenetic excitation of SST preBötC neurons evokes frequent doublet-shaped
895 sighs in ketamine/xylazine mice, while in awake mice it induces frequent sighs of augmented
896 breath shape, suggesting that doublets are indeed sighs.
897

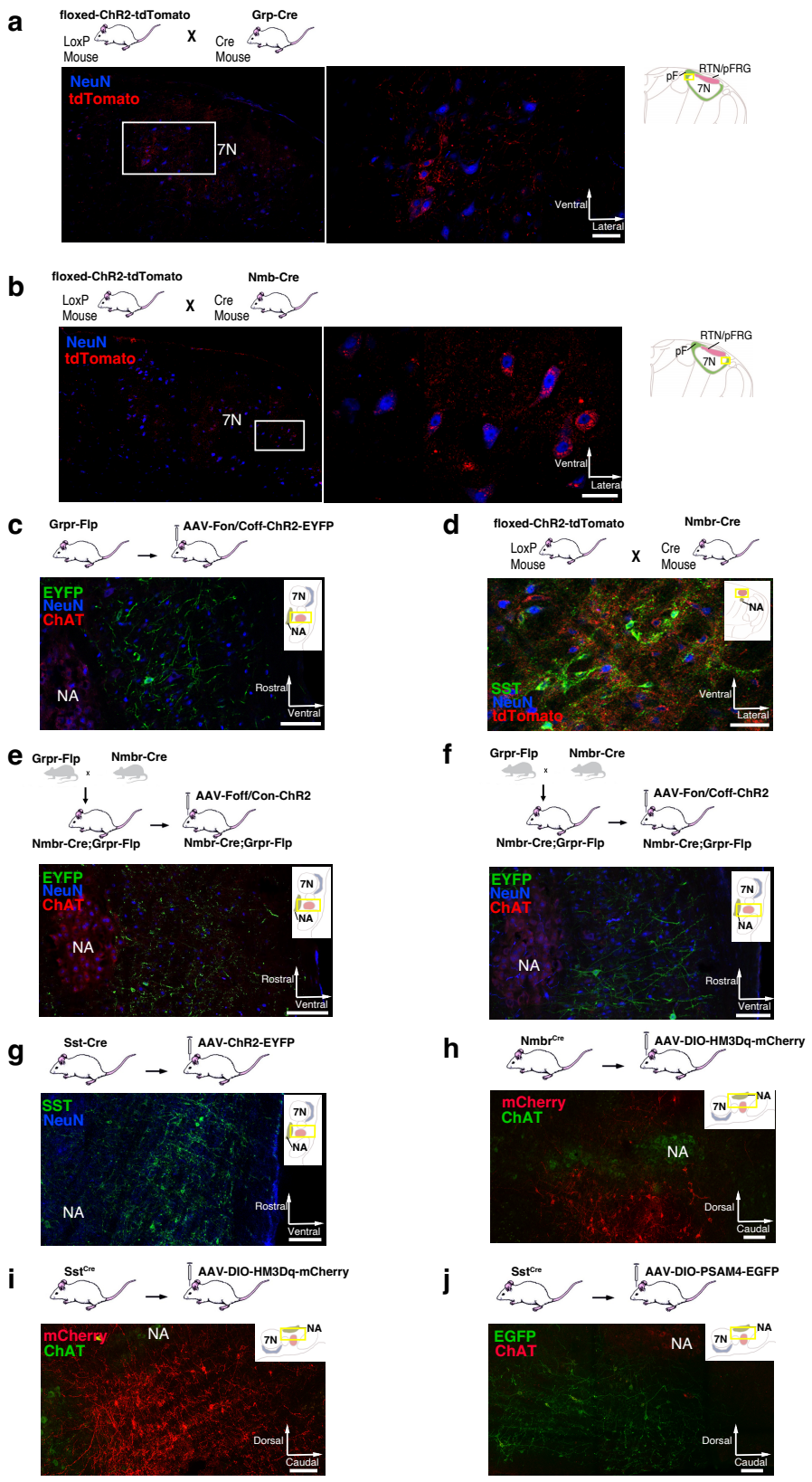
a
floxed-ChR2-tdTomato
LoxP Mouse
x
Grp-Cre
Cre Mouse
NeuN
tdTomato
7N
Ventral
Lateral
RTN/pFRG
pF
7N
b
floxed-ChR2-tdTomato
LoxP Mouse
x
Nmb-Cre
Cre Mouse
NeuN
tdTomato
7N
Ventral
Lateral
RTN/pFRG
pF
7N
c
Grpr-Flp
AAV-Fon/Coff-ChR2-EYFP
EYFP
NeuN
ChAT
7N
NA
NA
Rostral
Ventral
d
floxed-ChR2-tdTomato
LoxP Mouse
x
Nmbr-Cre
Cre Mouse
NA
SST
NeuN
tdTomato
Ventral
Lateral
e
Grpr-Flp
Nmbr-Cre
Nmbr-Cre;Grpr-Flp
AAV-Foff/Con-ChR2
Nmbr-Cre;Grpr-Flp
EYFP
NeuN
ChAT
7N
NA
NA
Rostral
Ventral
f
Grpr-Flp
Nmbr-Cre
Nmbr-Cre;Grpr-Flp
AAV-Fon/Coff-ChR2
Nmbr-Cre;Grpr-Flp
EYFP
NeuN
ChAT
7N
NA
NA
Rostral
Ventral
g
Sst-Cre
AAV-ChR2-EYFP
SST
NeuN
7N
NA
NA
Rostral
Ventral
h
Nmbr^Cre
AAV-DIO-HM3Dq-mCherry
mCherry
ChAT
7N
NA
NA
Dorsal
Caudal
i
Sst^Cre
AAV-DIO-HM3Dq-mCherry
mCherry
ChAT
NA
7N
NA
Dorsal
Caudal
j
Sst^Cre
AAV-DIO-PSAM4-EGFP
EGFP
ChAT
NA
7N
NA
Dorsal
Caudal

899 **Extended data Fig. 2. a,** tdTomato (red) in the pF neurons (blue) of Grp-ChR2 mice. Left:
900 Coronal brainstem section at the level of pF. Right: High-magnification micrographs of square
901 segment in left panel show ChR2 expression (tdTomato, red) in pF GRP neurons. Section also
902 labeled for NeuN (blue) immunoreactivity. Scale bar, 50 μm. **b,** tdTomato (red) in the pF
903 neurons (blue) of Nmb-ChR2 mice. Left: Coronal brainstem section at the level of pF. Right:
904 High-magnification micrographs of square segment in left panel show ChR2 expression
905 (tdTomato, red) in pF NMB neurons. Section also labeled for NeuN (blue) immunoreactivity.
906 Scale bar, 50 μm. **c,** Representative confocal micrograph of sagittal medullary section
907 (rectangle segment in inset panel) of $Grpr^{Flp}$ mice at the level of preBötC shows Flp-dependent
908 ChR2 expression (EYFP, green) targeted to preBötC GRPR neurons. ChR2-EYFP expression
909 was detectable in preBötC neurons 4 weeks after viral injection, with some expression in neuron
910 axons outside the preBötC including in the BötC rostral to the preBötC; in the intermediate
911 reticular formation (IRt) ventral to the Amb. We found very few ChR2-EYFP expressed axons in
912 neighboring ventral respiratory column (VRC) caudal to the preBötC, or at more distant
913 brainstem sites, e.g., 7N. No evidence of transfected neuron soma was found outside the
914 preBötC. Section also labeled for ChAT (red) and NeuN (blue) immunoreactivity. Scale bar,
915 100 μm. **d,** Representative confocal micrograph of coronal medullary section (rectangle
916 segment in inset panel) of transgenic Nmbr-ChR2 mice at the level of preBötC shows ChR2
917 expression (tdTomato, red) in preBötC NMBR neurons. ChR2- tdTomato expression was
918 detectable in the preBötC neurons, plus scattered neurons outside the preBötC including in the
919 intermediate reticular formation (IRt) ventral to the Amb and the gigantocellular reticular nucleus
920 (Gi) dorsomedial to the preBötC. Section also labeled for SST (green) and NeuN (blue)
921 immunoreactivity. Scale bar, 50 μm. **e,** Representative confocal micrograph of sagittal medullary
922 section (rectangle segment in inset panel) of $Nmbr^{Cre}$;$Grpr^{Flp}$ double mutant mice at the level of
923 preBötC shows ChR2 expression (EYFP, green) targeted to preBötC NMBR-only neurons.
924 ChR2-EYFP expression was detectable in preBötC neurons 4 weeks after viral injection, with
925 some expression in neuron axons in the BötC. No evidence of transfected neuron soma was
926 found outside the preBötC. Section also labeled for ChAT (red) and NeuN (blue)

927 immunoreactivity. Scale bar, 100 μm. **f,** Representative confocal micrograph of sagittal
928 medullary section (rectangle segment in inset panel) of $Nmbr^{Cre}$;$Grpr^{Flp}$ double mutant mice at
929 the level of preBötC shows ChR2 expression (EYFP, green) targeted to preBötC GRPR-only
930 neurons. ChR2-EYFP expression was detectable in preBötC neurons 4 weeks after viral
931 injection, with very little expression in neuron axons in neighboring area outside the preBötC. No
932 evidence of transfected neuron was found outside the preBötC. Section also labeled for ChAT
933 (red) and NeuN (blue) immunoreactivity. Scale bar, 100 μm. **g,** Representative confocal
934 micrograph of sagittal medullary section (rectangle segment in inset panel) of Sst^{Cre} mice at the
935 level of preBötC shows Cre-dependent ChR2 expression (EYFP, green) targeted to preBötC
936 SST neurons. ChR2-EYFP expression was detectable in preBötC neurons 4 weeks after viral
937 injection, with some expression in neighboring neurons outside the preBötC including in the
938 BötC rostral to the preBötC. The peak density of transfected neurons was caudal to the BötC
939 and ventral to the Amb. We found no evidence of transfected neurons at more distant brainstem
940 sites. Section also labeled for NeuN (blue) immunoreactivity. Scale bar, 100 μm. **h,**
941 Representative confocal micrograph of sagittal medullary section (rectangle segment in inset
942 panel) of $Nmbr^{Cre}$ mice at the level of preBötC shows Cre-dependent HM3Dq expression
943 (mCherry, red) targeted to preBötC NMBR neurons. HM3Dq-mCherry expression was
944 detectable in preBötC neurons 4 weeks after viral injection, with the highest density of
945 transfected somas in the preBötC. No evidence of transfected neuron was found outside
946 preBötC. Section also labeled for ChAT (green) immunoreactivity. Scale bar, 100 μm. **i,**
947 Representative confocal micrograph of sagittal medullary section (rectangle segment in inset
948 panel) of SST^{Cre} mice at the level of preBötC shows Cre-dependent HM3Dq expression
949 (mCherry, red) targeted to preBötC SST neurons. HM3Dq-mCherry expression was detectable
950 in preBötC neurons 4 weeks after viral injection, with the highest density of transfected somas in
951 the preBötC and minimal (<10% of transfected somas) found outside of preBötC. Section also
952 labeled for ChAT (green) immunoreactivity. Scale bar, 100 μm. **j,** Representative confocal
953 micrograph of sagittal medullary section (rectangle segment in inset panel) of SST^{Cre} mice at the
954 level of preBötC shows Cre-dependent PSAM4 expression (EGFP, green) targeted to preBötC

955 SST neurons. PSAM4-EGFP expression was detectable in preBötC neurons 4 weeks after viral
956 injection, with the highest density of transfected somas in the preBötC and minimal (<10% of
957 transfected somas) found outside of preBötC. Section also labeled for ChAT (red)
958 immunoreactivity. Scale bar, 100 μm.
959

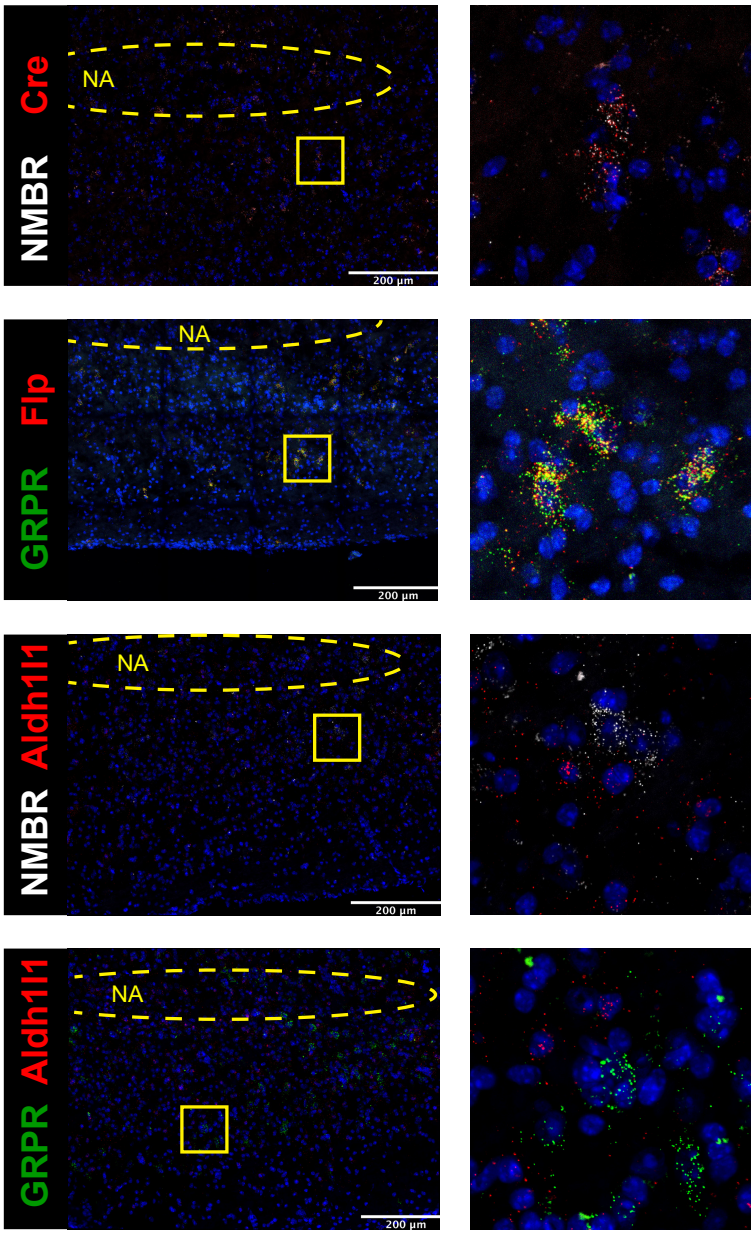

960

961 **Extended data Fig. 3.** Colocalization between NMBR and Cre (A) and GRPR and Flp (B). All

962 NMBR neurons expressed transcripts for Cre in brainstem tissue from $Nmbr^{Cre}$ mice and all

963 GRPR neurons expressed transcripts for Flp in brainstem tissue from $Grpr^{Flp}$ mice.

964 Colocalization between transcripts for NMBR, GRPR and astrocytic marker Aldh1l1 (C-D).

965 Aldh1l1 was expressed throughout the brain tissue, with no clear boundaries demarking cells;

966 therefore, we used NMBR and GRPR expression to determine cells boundaries and then
967 assessed presence of Aldh1l1 within those boundaries. Vast majority of $NMBR^+$ and $GRPR^+$
968 neurons (97%) did not contain transcripts for Aldh1l1. NA: Nucleus ambiguous, location was
969 determined using ChAT probe. Yellow squares indicate zoomed images (right, 100x100μm)
970

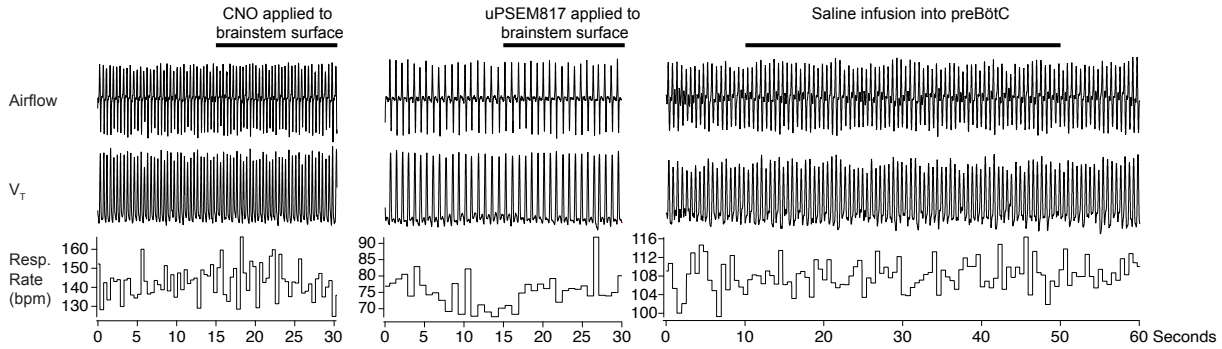

Extended data Fig. 4. Control applications of CNO, uPSEM817 or Saline. We confirmed that application of CNO (left), uPSEM817 (middle) or saline infusion into preBötC did not evoke changes in breathing parameters and do not evoke sighing.

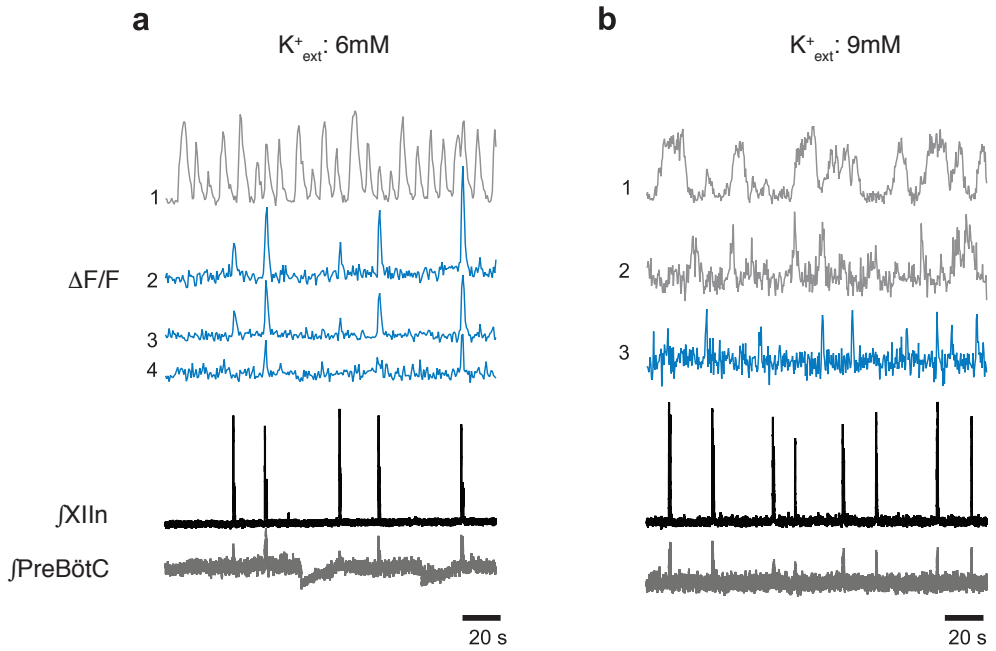

Extended data Fig. 5. Examples of Ca^{2+} oscillations *in vitro* in phase with inspiratory rhythm (blue) and out of phase (gray) in a) 6 mM $[K^+]_{ext}$ (four neurons) and b) 9 mM $[K^+]_{ext}$ (three neurons).

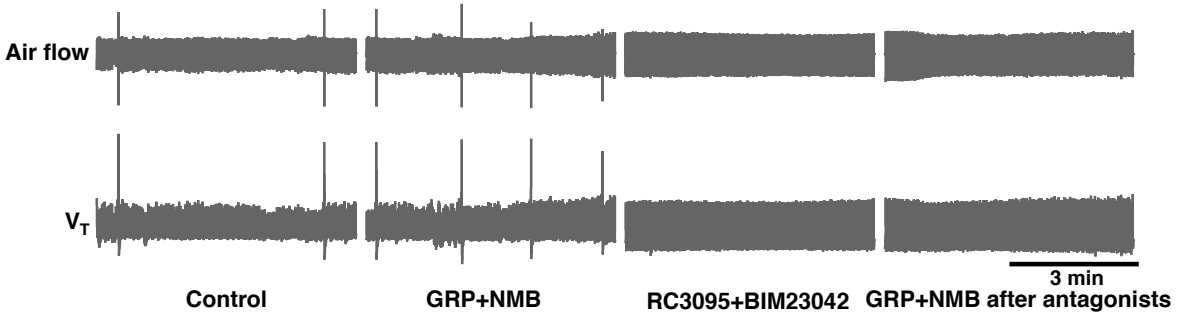

Extended data Fig. 6. GRP and NMB receptors in preBötC effectively blocked by RC3095+BIM23042 microinjections. RC3095 and BIM23042 effectively blocked GRPRs and NMBRs, as respiratory responses induced by GRP and NMB microinjection into the preBötC, sufficient to increase sigh rate by 585 ± 209% of control, were fully antagonized by the same concentration of RC3095 and BIM23042 (n = 3). Air flow and V_T traces show the changes in sigh rate under different conditions (from left to right) in anesthetized mice (note sighs are evident as single events significantly larger than normal breaths): control; GRP+NMB: after bilateral injection of GRP+NMB into preBötC; RC3095+BIM23042: after bilateral injection of RC3095+BIM23042 (300 μM each, 50-60 nl/side) into preBötC; GRP+NMB after antagonists: the second bilateral injection of GRP+NMB, i.e., same dose of GRP+NMB that resulted in the higher sigh rate before RC3095+BIM23042 did not induce sighing after the antagonist injection.

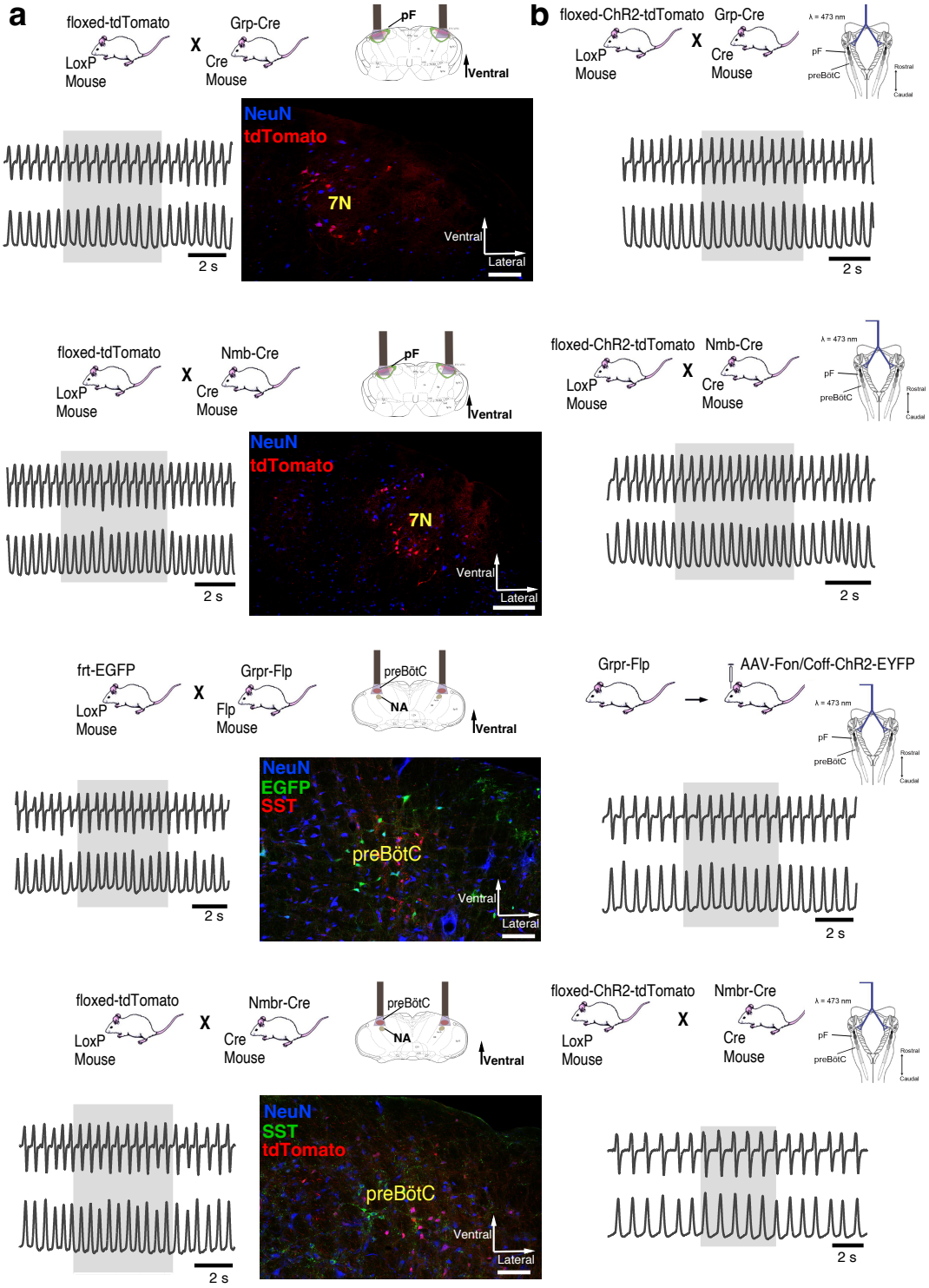
a
floxed-tdTomato
LoxP Mouse
X
Grp-Cre
Cre Mouse
pF
Ventral
NeuN
tdTomato
7N
Ventral
Lateral
2 s
b
floxed-ChR2-tdTomato
LoxP Mouse
X
Grp-Cre
Cre Mouse
λ = 473 nm
pF
preBötC
Rostral
Caudal
2 s
floxed-tdTomato
LoxP Mouse
X
Nmb-Cre
Cre Mouse
pF
Ventral
NeuN
tdTomato
7N
Ventral
Lateral
2 s
floxed-ChR2-tdTomato
LoxP Mouse
X
Nmb-Cre
Cre Mouse
λ = 473 nm
pF
preBötC
Rostral
Caudal
2 s
frt-EGFP
LoxP Mouse
X
Grpr-Flp
Flp Mouse
preBötC
NA
Ventral
NeuN
EGFP
SST
preBötC
Ventral
Lateral
2 s
Grpr-Flp
AAV-Fon/Coff-ChR2-EYFP
λ = 473 nm
pF
preBötC
Rostral
Caudal
2 s
floxed-tdTomato
LoxP Mouse
X
Nmbr-Cre
Cre Mouse
preBötC
NA
Ventral
NeuN
SST
tdTomato
preBötC
Ventral
Lateral
2 s
floxed-ChR2-tdTomato
LoxP Mouse
X
Nmbr-Cre
Cre Mouse
λ = 473 nm
pF
preBötC
Rostral
Caudal
2 s

995 **Extended data Fig. 7. a,** No output effects and no sigh were produced by pF or preBötC
996 photostimulation in (from top to bottom) Grp-RFP, Nmb-RFP, Grpr-EGFP and Nmbr-RFP
997 reporter mice. **b,** Stimulating 500 μm rostral to pF or preBötC in ChR2 expressed mice (from top
998 to bottom: Grp-ChR2, Nmb-ChR2, Grpr-Flp and Nmbr-ChR2 mice) did not produce
999 significant output effects.
1000

1001 References

1002 1. Knowlton, G.C. & Larrabee, M.G. A unitary analysis of pulmonary volume receptors. *Am*
1003 *J Physiol* **147**, 100-114 (1946).

1004 2. McCutcheon, F.H. Atmospheric respiration and the complex cycles in mammalian
1005 breathing mechanisms. *J Cell Comp Physiol* **41**, 291-303 (1953).

1006 3. Reynolds, L.B., Jr. Characteristics of an inspiration-augmenting reflex in anesthetized
1007 cats. *J Appl Physiol* **17**, 683-688 (1962).

1008 4. Li, P.*, et al.* The peptidergic control circuit for sighing. *Nature* **530**, 293-297 (2016).

1009 5. Li, P.*, et al.* Brain Circuit of Claustrophobia-like Behavior in Mice Identified by Upstream
1010 Tracing of Sighing. *Cell Rep* **31**, 107779 (2020).

1011 6. Ramirez, J.M. The integrative role of the sigh in psychology, physiology, pathology, and
1012 neurobiology. *Prog Brain Res* **209**, 91-129 (2014).

1013 7. Li, P. & Yackle, K. Sighing. *Curr Biol* **27**, R88-r89 (2017).

1014 8. Cui, Y.*, et al.* Defining preBötzinger Complex Rhythm- and Pattern-Generating Neural
1015 Microcircuits In Vivo. *Neuron* **91**, 602-614 (2016).

1016 9. Shi, Y.*, et al.* Neuromedin B Expression Defines the Mouse Retrotrapezoid Nucleus. *J*
1017 *Neurosci* **37**, 11744-11757 (2017).

1018 10. Fenno, L.E.*, et al.* Targeting cells with single vectors using multiple-feature Boolean
1019 logic. *Nat Methods* **11**, 763-772 (2014).

1020 11. Smith, J.C., Ellenberger, H.H., Ballanyi, K., Richter, D.W. & Feldman, J.L. Pre-Bötzinger
1021 complex: a brainstem region that may generate respiratory rhythm in mammals. *Science*
1022 **254**, 726-729 (1991).

1023 12. Gray, P.A., Rekling, J.C., Bocchiaro, C.M. & Feldman, J.L. Modulation of respiratory
1024 frequency by peptidergic input to rhythmogenic neurons in the preBötzinger complex.
1025 *Science* **286**, 1566-1568 (1999).

1026 13. Feldman, J.L. & Kam, K. Facing the challenge of mammalian neural microcircuits: taking
1027 a few breaths may help. *J Physiol* **593**, 3-23 (2015).

1028 14. Ashhad, S. & Feldman, J.L. Emergent Elements of Inspiratory Rhythmogenesis: Network
1029 Synchronization and Synchrony Propagation. *Neuron* **106**, 482-497 e484 (2020).

1030 15. Fenno, L.E.*, et al.* Comprehensive Dual- and Triple-Feature Intersectional Single-Vector
1031 Delivery of Diverse Functional Payloads to Cells of Behaving Mammals. *Neuron* **107**,
1032 836-853 e811 (2020).

1033 16. Magnus, C.J.*, et al.* Ultrapotent chemogenetics for research and potential clinical
1034 applications. *Science* **364**(2019).

17. Carnevali, L.*, et al.* Different patterns of respiration in rat lines selectively bred for high or low anxiety. *PLoS One* **8**, e64519 (2013).

18. Del Negro, C.A., Funk, G.D. & Feldman, J.L. Breathing matters. *Nat Rev Neurosci* **19**, 351-367 (2018).

19. Kam, K., Worrell, J.W., Janczewski, W.A., Cui, Y. & Feldman, J.L. Distinct inspiratory rhythm and pattern generating mechanisms in the preBötzinger complex. *J Neurosci* **33**, 9235-9245 (2013).

20. Sherman, D., Worrell, J.W., Cui, Y. & Feldman, J.L. Optogenetic perturbation of preBötzinger complex inhibitory neurons modulates respiratory pattern. *Nat Neurosci* **18**, 408-414 (2015).

21. Lieske, S.P., Thoby-Brisson, M., Telgkamp, P. & Ramirez, J.M. Reconfiguration of the neural network contrlling multiple breathing patterns: eupnea, sighs and gasps. *Nat. Neurosci.* **6**, 600-607 (2000).

22. Feldman, J.L. & Gray, P.A. Sighs and gasps in a dish. *Nat Neurosci* **3**, 531-532 (2000).

23. de Sousa Abreu, R.P., Bondarenko, E. & Feldman, J.L. Phase- and state-dependent modulation of breathing pattern by preBotzinger complex somatostatin expressing neurons. *J Physiol* **600**, 143-165 (2022).

24. Cherniack, N.S., von Euler, C., Głogowska, M. & Homma, I. Characteristics and rate of occurrence of spontaneous and provoked augmented breaths. *Acta Physiol Scand* **111**, 349-360 (1981).

25. Janczewski, W.A., Pagliardini, S., Cui, Y. & Feldman, J.L. Sighing after vagotomy. in *Society for Neuroscience* (New Orleans, 2012).

26. Borrus, D.S.*, et al.* Inspiratory and sigh breathing rhythms depend on distinct cellular signalling mechanisms in the preBötzinger complex. *J Physiol* (2024).

27. Chapuis, C., Autran, S., Fortin, G., Simmers, J. & Thoby-Brisson, M. Emergence of sigh rhythmogenesis in the embryonic mouse. *J Physiol* **592**, 2169-2181 (2014).

28. Kamichi, S.*, et al.* Immunohistochemical localization of gastrin-releasing peptide receptor in the mouse brain. *Brain Res* **1032**, 162-170 (2005).

29. Kaczyńska, K. & Szereda-Przestaszewska, M. Peripheral cardiorespiratory effects of bombesin in anaesthetized rats. *Eur J Pharmacol* **602**, 157-162 (2009).